

# Calculation of the Linear-Absorption Spectrum of an Ideal Two-Dimensional System of $\text{MoS}_2$

Dissertation  
For the award of the Bachelor degree  
in Natural Science

Vo Chau Duc Phuong  
Department of Theoretical Physics  
Faculty of Physics-Engineering Physics  
University of Science  
National University of Science Vietnam  
Ho Chi Minh city (July 2024)

## Commitment

I commit to independently conducting the calculation of the linear-absorption spectrum of an ideal two-dimensional system of **MoS<sub>2</sub>** for my bachelor thesis, under the supervision of Dr. Huynh Thanh Duc, and with guidance from Master Le Minh Chau.

## Acknowledgments

# Contents

<b>1</b>	<b>Introduction</b>	<b>6</b>
1.1	Overview of Two Dimensional Material Research . . . . .	6
1.2	Methods and Results . . . . .	6
1.3	Overview on Theories . . . . .	7
<b>2</b>	<b>Theories</b>	<b>8</b>
2.1	Tight-Binding Theories . . . . .	8
2.2	Three Band Tight-Binding Model . . . . .	9
2.3	System Hamiltonian . . . . .	12
2.3.1	First Quantization Hamiltonian . . . . .	12
2.3.2	Second Quantization Hamiltonian . . . . .	13
2.4	Semiconductor Bloch Equation . . . . .	14
2.5	Polarization Density . . . . .	15
<b>3</b>	<b>Numerical Methods</b>	<b>16</b>
3.1	Numerical Sum Over k-Space . . . . .	16
3.2	Cut Off K-point Technique . . . . .	17
3.3	Numerical Analyzing . . . . .	18
<b>4</b>	<b>Results and Discussion</b>	<b>19</b>
<b>5</b>	<b>Conclusion and Further</b>	<b>22</b>
	<b>Appendices</b>	<b>i</b>
<b>A</b>	<b>Electromagnetic Field - Charge Interaction Hamiltonian</b>	<b>i</b>
<b>B</b>	<b>Electron - Electron Interaction Hamiltonian</b>	<b>ii</b>
<b>C</b>	<b>Motion Equation</b>	<b>iv</b>
<b>D</b>	<b>Dipole Matrix Elements</b>	<b>vi</b>

## List of Figures

1	TMD structure and its first Brillouin zone . . . . .	9
2	Band structure of $\text{MoS}_2$ material along $M \rightarrow -K \rightarrow \Gamma \rightarrow K \rightarrow M$ direction . . . . .	11
3	Rhombus primitive unit cell in compare with hexagon primitive unit cell (the first Brillouin zone) . . . . .	16
4	New Basics Based on the rhombus unit vectors . . . . .	17
5	k-radius show the cutoff circle around $K'$ points . . . . .	17
6	Electric field on Ox direction and it Fourier Transform . . . . .	18
7	Measured absorption spectrum of $\text{MoS}_2$ . . . . .	19
8	Absorption Spectrum with difference $T_2$ . . . . .	20
9	Absorption Spectrum with difference dielectric $\epsilon$ and without Coulomb interaction . .	21
10	Absorption Spectrum with difference number of k-points . . . . .	21

## List of Tables

1	Fitting parameters in three-band tight-binding model for $\text{MoS}_2$ . . . . .	11
2	Exciton binding energy with difference dielectric . . . . .	19

# Thesis Information

Name of Thesis: Calculation of the Linear-Absorption Spectrum of MoS<sub>2</sub>

Major: Theoretical Physics

Student's name: Vo Chau Duc Phuong

Year: 2020-2024

Supervisor: Dr. Huynh Thanh Duc

Department: Theoretical of Physics

Faculty: Physics - Engineering Physics

University: University of Science

## Abstract

Transition Metal Dichalcogenides (TMD) are promising semiconductors due to their extraordinary electronic and optoelectronic properties. Before calculating the nonlinear optical properties of this material, we need to calculate the linear absorption spectrum. In monolayer TMD, the Coulomb interaction heavily influences the increase in exciton binding energies. Therefore, the independent electron approximation model is not reliable for simulating the experiment, especially in low-dimensional systems. In this work, we use a minimum three-band Tight-Binding Hamiltonian for the band structure calculation and the Semiconductor Bloch Equation to model the response of electron density in MoS<sub>2</sub> material to a laser over time to calculate the Linear Absorption Spectra (LAS) and extract the Exciton binding energy from it. Our calculation on exciton binding energy (0.24 eV) based on this model proves to be more accurate than some previous theoretical, which predict exciton binding energy too large (0.5-1 eV). From this work, we can use it to calculate other effects which affected by Exciton binding energy such as photo-current, high harmonic generation, and high-order sideband generation.

# 1 Introduction

## 1.1 Overview of Two Dimensional Material Research

The researcher has dedicated many years to studying Graphene, with hopes that it could potentially serve as the new silicon, enabling the continuation of Moore’s law on the CPU chip dice. However, in recent years, a number of papers on Graphene properties has reached thousands yearly, indicating that research on ‘simple graphene’ has peaked.<sup>1</sup> Therefore, the researchers shifted their focus from working solely with Graphene to exploring applications and other two-dimensional materials.

Atomically thin two-dimensional (2D) forms of layered transition metal dichalcogenides (TMD) have recently gained significant scientific and technological interest since the first five years of the Graphene boom.<sup>1;2</sup> TMD has the chemical composition  $MX_2$ , so it has a wide range of materials. They include both metals and semiconductors, for example  $NbS_2$ ,  $NbSe_2$ ,  $TaS_2$ ,  $TaSe_2$ ,  $\beta$ - $MoT_2$  and  $Td-WTe_2$  are bulk metals while the  $ReS_2$ ,  $ZrS_2$ ,  $MoS_2$ ,  $WS_2$ ,  $MoSe_2$ ,  $WSe_2$  and  $\alpha$ - $MoTe_2$  are semiconductors. The structure of TMD consists of multiple monolayers bonded by van der Waals forces, with in-plane stability ensured by strong covalent bonds. Among various transition metal dichalcogenides, the group-VIB ( $M = Mo, W$ ;  $X = S, Se$ ) is stable in both mono- and few-layers in the air at room temperature.<sup>1</sup> These two-dimensional semiconductors have a direct band gap in the visible frequency range, stable and excellent mobility at room temperature<sup>2;3</sup>, and promise to become a good candidate for electronic and optoelectronic applications.

Transition metal dichalcogenides (TMD) exhibit non-centrosymmetry, resulting in unique properties in electronic and valleytronic applications. These are characterized by valley-dependent optical transitions<sup>4;5</sup>. Additionally, significant Spin-Orbit Coupling in TMD creates a considerable split in the band structure valley. The low dimension system cause the reduced screening of Coulomb interaction outside the monolayer’s plane, resulting in large exciton binding energies<sup>6;7</sup>. These binding energies are notably higher than those observed in typical III-V materials, implying that many-body interactions play a key role in determining the electronic and optical properties of these materials. Previous theoretical works have predict the binding energy too large<sup>8–11</sup> when compare with experiment<sup>7</sup> and other more accurate theoretical works<sup>6;7</sup>.

## 1.2 Methods and Results

In our current research, our main objective is to identify the most appropriate model for estimating the exciton or trion binding energy while aligning with experimental data. The key challenge is to identify a model that strikes a balance between simplicity and accuracy. Our primary focuses on investigating the properties of transition metal dichalcogenides (TMD). Several models, such as ab initio calculations<sup>6;8–11</sup> and parabola approximation<sup>12;13</sup>, have been developed and employed to simulate the band structure. It is important to note that these models have limitations as they can only calculate around highly symmetric points and not across the entire Brillouin zone (BZ). In our study, we are using a three-band tight-binding model to calculate properties across the entire BZ, which should give us results that better match experimental data.

From now and for later in this work, we use the minimal three-band tight-binding Hamiltonian<sup>14</sup> to calculate the band structure by determining the eigenvalues at each k-point. The momentum matrix for the velocity gauge matrix will be calculated using finite differentiation, and then utilized to compute the dipole matrix. We plan to solve the Semiconductor Bloch Equations (SBE) using the RungeKutta 4th order method to numerically find the time-independent density evolution. Based on this density, we can derive the polarization, current density, and other measurable physical parameters. After obtaining the polarization, we will perform a Fourier transform to obtain the

absorption spectrum.

In our analysis, we concentrated on the low excitation regime to examine the linear absorption spectra. We were able to concentrate on scenarios where the electron density in the conduction bands is significantly lower than that in the valence bands. The results showed a significant exciton binding energy, which closely matched both experimental measurements and theoretical expectations. These discoveries allow us to predict the existence of smaller excitons and use the binding energy to investigate other effects influenced by the Coulomb interaction. We were able to concentrate on scenarios where the electron density in the conduction bands is significantly lower than that in the valence bands. The results showed a significant exciton binding energy, which closely matched both experimental measurements and theoretical expectations. These discoveries allow us to predict the existence of smaller excitons and use the binding energy to investigate other effects influenced by the Coulomb interaction.

### 1.3 Overview on Theories

The theoretical part includes the following topics:

- Theory on the Tight-Binding Approximation: Starting from the Schrödinger equation for the independent charge approximation with the LCAO ansatz. Show the on-site and hopping energies, as well as the overlap densities parameters for the semi-empirical formalism.
- Derivation of light-matter interaction for charge systems, using the velocity gauge.
- Derivation of Semiconductor Bloch Equation in the Hatree-Fock approximation (HFA), along with the dephasing  $T_2$  approximation.
- Steps to numerically calculate the polarization density and linear absorption spectrum.



## 2 Theories

### 2.1 Tight-Binding Theories

We start from Hamiltonian  $H$  for many-body system in the independent electron approximation:

$$H = \sum_{\lambda} H^{1e}(\mathbf{r}_{\lambda}). \quad (1)$$

In the independent electron approximation, the stationary state of an electron in a solid is presented by the one-particle time-independent Schrödinger equation:

$$H_{1e}\psi_{\lambda\mathbf{k}}(\mathbf{r}) = \left( -\frac{\hbar^2\nabla^2}{2m} + V_0(\mathbf{r}) \right) \psi_{\lambda\mathbf{k}}(\mathbf{r}) = \varepsilon_{\lambda}(\mathbf{k})\psi_{\lambda\mathbf{k}}(\mathbf{r}). \quad (2)$$

We assume that the electrons stay close to the atomic sites and that the electronic wave functions centered around neighboring sites have little overlap. There is almost no overlap between wave functions for electrons that are separated by two or more atoms. Therefore, the wave function of an electron will have the similar form of atomic orbital and we can describe it in the form of Linear Combination of Atomic Orbitals (LCAO):

$$\psi(\mathbf{r}) = \sum_{n=1}^N \sum_{c=1}^{N_c} \sum_{\alpha=1}^{N_{orb}} c_{\alpha c}(\mathbf{R}_n) \phi_{\alpha}(\mathbf{r} - \mathbf{R}_n - \mathbf{r}_c). \quad (3)$$

In which  $\phi_{\alpha}$  is orbital wave function of an atomic,  $\mathbf{R}_n$  is position of Bravais unit cell,  $\mathbf{r}_c$  is relative position of the atom in that cell,  $N_{orb}$  is number of orbital of an atom,  $N_c$  is number of atom in a unit cell and  $N$  is the number of unit cell in the lattice. Based on LCAO wave function, we can construct the Bloch wave function in the following form:

$$\psi_{\mathbf{k}}(\mathbf{r}) = \sum_{c=1}^{N_c} \sum_{\alpha=1}^{N_{orb}} C_{\alpha c}(\mathbf{k}) \sum_{n=1}^N e^{i\mathbf{k}(\mathbf{R}_n + \mathbf{r}_c)} \phi_{\alpha}(\mathbf{r} - \mathbf{R}_n - \mathbf{r}_c) \quad (4)$$

This wave function satisfies the Bloch theorem. Include (4) in the one-particle time-dependent Schrödinger equation (2), multiply with  $e^{i\mathbf{k}'\mathbf{r}'}\phi_{\alpha'}^*(\mathbf{r} - \mathbf{r}_{c'})$  on the left, and take the integral over  $\mathbf{r}$  to have:

$$\sum_{c=1}^{N_c} \sum_{\alpha=1}^{N_{orb}} (H_{\alpha'c',\alpha c}(\mathbf{k}) - \varepsilon(\mathbf{k})S_{\alpha'c',\alpha c}(\mathbf{k}))C_{\alpha c}(\mathbf{k}) = 0. \quad (5)$$

In which on-site hopping energies  $H_{\alpha'c',\alpha c}(\mathbf{k})$  and overlap density  $S_{\alpha'c',\alpha c}(\mathbf{k})$  defined by:

$$H_{\alpha'c',\alpha c}(\mathbf{k}) = \sum_{n=1}^N e^{i\mathbf{k}(\mathbf{R}_n + \mathbf{r}_c - \mathbf{r}_{c'})} \int d\mathbf{r} \phi_{\alpha'}^*(\mathbf{r} - \mathbf{r}_{c'}) H_{1e} \phi_{\alpha}(\mathbf{r} - \mathbf{R}_n - \mathbf{r}_c), \quad (6)$$

$$S_{\alpha'c',\alpha c}(\mathbf{k}) = \sum_{n=1}^N e^{i\mathbf{k}(\mathbf{R}_n + \mathbf{r}_c - \mathbf{r}_{c'})} \int d\mathbf{r} \phi_{\alpha'}^*(\mathbf{r} - \mathbf{r}_{c'}) \phi_{\alpha}(\mathbf{r} - \mathbf{R}_n - \mathbf{r}_c). \quad (7)$$

Solving the eq. (5) in several  $k$ -point, we will have the wave functions and energy. In the semi-empirical formalism, these integrals shall be left as phenomenological parameters. By finding the eigenvalues of this Hamiltonian at every  $k$ -point, we can construct the band structure for the system.

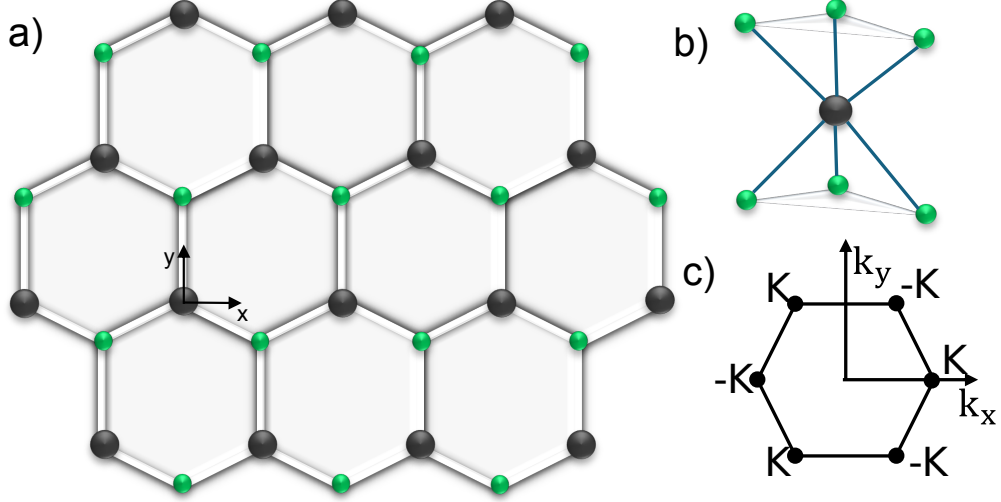


Figure 1: (a) Top view of monolayer MX<sub>2</sub>. The large sphere is **M** and the small sphere is X. (b) sideview of monolayer MX<sub>2</sub>. (c) The 2D first Brillouin zone with special k points.

## 2.2 Three Band Tight-Binding Model

In previous ab initio calculations<sup>15–19</sup>, Prof. Xiao and his colleague discovered that the monolayer of MX<sub>2</sub> with  $D_{3h}$  point-group symmetry has a structure as shown in Figure 1. They found that the Bloch states of the monolayer MoS<sub>2</sub> near the band edges are primarily composed of Mo-d orbitals, particularly the  $d_{z^2}$ ,  $d_{xy}$ , and  $d_{x^2-y^2}$  orbitals. To accurately capture the band-edge properties in the  $K$  and  $K'$  valleys, they developed an approximate model for group VII-B TMD consisting of only these three bands and neglecting  $X-p$  orbitals, and then extended it to fit the entire Brillouin Zone<sup>14</sup>.

Denote three M-d bands as:

$$|\phi_1\rangle = d_{z^2}, \quad |\phi_2\rangle = d_{xy}, \quad |\phi_3\rangle = d_{x^2-y^2}. \quad (8)$$

As discussed above, the Bloch states near the band edges mostly consist of Mo-d orbital, therefore we ignore the  $\mathbf{r}_c$  and the sum over it in hopping energy (6). Each pair of difference bases is assumed to be orthogonal; therefore the overlapping matrix element become:

$$S_{\alpha,\alpha'}(\mathbf{k}) = \delta_{\alpha\alpha'}.$$

The hopping energies eq.(6) between the atomic orbitals  $|\phi_\mu\rangle$  at 0 and  $|\phi_{\mu'}\rangle$  at lattice vector  $\mathbf{R}$  can be obtained as:

$$H_{\mu\mu'}(\mathbf{k}) = \sum_{\mathbf{R}} e^{i\mathbf{k}\cdot\mathbf{R}} \langle \phi_\mu(\mathbf{r}) | \hat{H} | \phi_{\mu'}(\mathbf{r} - \mathbf{R}) \rangle.$$

Confined by the symmetry of the system, Tight-binding Hamiltonian have the form:

$$H^{TNN}(\mathbf{k}) = \begin{pmatrix} V_0 & V_1 & V_2 \\ V_1^* & V_{11} & V_{12} \\ V_2^* & V_{12}^* & V_{22} \end{pmatrix}, \quad (9)$$

where

$$\begin{aligned}
V_0 &= \varepsilon_1 + 2t_0(2\cos\alpha\cos\beta + \cos 2\alpha) + 2r_0(2\cos 3\alpha\cos\beta + \cos 2\beta), \\
\text{Re}[V_1] &= -2\sqrt{3}t_2\sin\alpha\sin\beta + 2(r_1 + r_2)\sin 3\alpha\sin\beta - 2\sqrt{3}u_2\sin 2\alpha\sin 2\beta, \\
\text{Im}[V_1] &= 2t_1\sin\alpha(2\cos\alpha + \cos\beta) + 2(r_1 - r_2)\sin 3\alpha\cos\beta + 2u_1\sin 2\alpha(2\cos 2\alpha + \cos 2\beta) \\
\text{Re}[V_2] &= 2t_2(\cos 2\alpha - \cos\alpha\cos\beta) - \frac{2}{\sqrt{3}}(r_1 + r_2)(\cos 3\alpha\cos\beta - \cos 2\beta) + 2u_2(\cos 4\alpha - \cos 2\alpha\cos 2\beta), \\
\text{Im}[V_2] &= 2\sqrt{3}t_1\cos\alpha\sin\beta + \frac{2}{\sqrt{3}}\sin\beta(r_1 - r_2)(\cos 3\alpha + 2\cos\beta), \\
V_{11} &= \varepsilon_2 + (t_{11} + 3t_{22})\cos\alpha\cos\beta + 2t_{11}\cos 2\alpha + 4r_{11}\cos 3\alpha\cos\beta \\
&\quad + 2(r_{11} + \sqrt{3}r_{12})\cos 2\beta + (u_{11} + 3u_{22})\cos 2\alpha\cos 2\beta + 2u_{11}\cos 4\alpha, \\
\text{Re}(V_{12}) &= \sqrt{3}(t_{22} - t_{11})\sin\alpha\sin\beta + 4r_{12}\sin 3\alpha\sin\beta + \sqrt{3}(u_{22} - u_{11})\sin 2\alpha\sin 2\beta, \\
\text{Im}[V_{12}] &= 4t_{12}\sin\alpha(\cos\alpha - \cos\beta) + 4u_{12}\sin 2\alpha(\cos 2\alpha - \cos 2\beta), \\
V_{22} &= \varepsilon_2 + (3t_{11} + t_{22})\cos\alpha\cos\beta + 2t_{22}\cos 2\alpha + 2r_{11}(2\cos 3\alpha\cos\beta + \cos 2\beta) \\
&\quad + \frac{2}{\sqrt{3}}r_{12}(4\cos 3\alpha\cos\beta - \cos 2\beta) + (3u_{11} + u_{22})\cos 2\alpha\cos 2\beta + 2u_{22}\cos 4\alpha,
\end{aligned}$$

and

$$(\alpha, \beta) = \left(\frac{1}{2}k_x a, \frac{\sqrt{3}}{2}k_y a\right), \quad (10)$$

11 additional parameters shown in table 1 obtained by fitting with FP calculation results. Due to the heavy transition-metal atom M, its Spin Orbit Coupling (SOC) can be larges. For simplicity, only the on-site contribution, namely, the  $\mathbf{L}\cdot\mathbf{S}$  term from M atoms, is considered. Using the base  $\{|d_{z^2}, \uparrow\rangle, |d_{xy}, \uparrow\rangle, |d_{x^2-y^2}, \uparrow\rangle, |d_{z^2}, \downarrow\rangle, |d_{xy}, \downarrow\rangle, |d_{x^2-y^2}, \downarrow\rangle\}$ , the contribution of SOC to the Hamiltonian can be written as

$$H' = \lambda \mathbf{L}\cdot\mathbf{S} = \frac{\lambda}{2} \begin{pmatrix} L_z & 0 \\ 0 & -L_z \end{pmatrix}. \quad (11)$$

In which,

$$L_z = \begin{pmatrix} 0 & 0 & 0 \\ 0 & 0 & 2i \\ 0 & -2i & 0 \end{pmatrix}, \quad (12)$$

is the matrix of  $\hat{L}_z$  (z component of the orbital angular momentum) in bases of  $d_{z^2}$ ,  $d_{xy}$  and  $d_{x^2-y^2}$ , and  $\lambda$  is characterized for the strength of the SOC. Under these bases, the matrix elements of  $\hat{L}_x$  and  $\hat{L}_y$  are all zeros. Therefore the Hamiltonian with SOC have the form:

$$H(\mathbf{k}) = H_{SOC}(\mathbf{k}) = I_2 \otimes H^{TNN}(\mathbf{k}) + H' = \begin{bmatrix} H(\mathbf{k}) + \frac{\lambda}{2}L_z & 0 \\ 0 & H_0(\mathbf{k}) - \frac{\lambda}{2}L_z \end{bmatrix}. \quad (13)$$

By finding eigenvalue of Hamiltonian  $H$  in each  $\mathbf{k}$  point on entire BZ, the bands structure will be obtained. The bands structure with the huge bands split at the K and K' point of MoS<sub>2</sub> is caused by SOC is shown in fig.2.

$\varepsilon_1$	$\varepsilon_2$	$t_0$	$t_1$	$t_2$	$t_{11}$	$t_{12}$	$t_{22}$	$r_0$	$r_1$
$r_2$	$r_{11}$	$r_{12}$	$u_0$	$u_1$	$u_2$	$u_{11}$	$u_{12}$	$u_{22}$	$\lambda$
0.820	1.931	-0.176	-0.101	0.531	0.084	0.169	0.070	0.070	-0.252
0.084	0.019	0.093	-0.043	0.047	0.005	0.304	-0.192	-0.162	0.073

Table 1: Fitting parameters in three-band tight-binding model for local-density approximation (LDA) cases for  $MoS_2$ .<sup>14</sup>

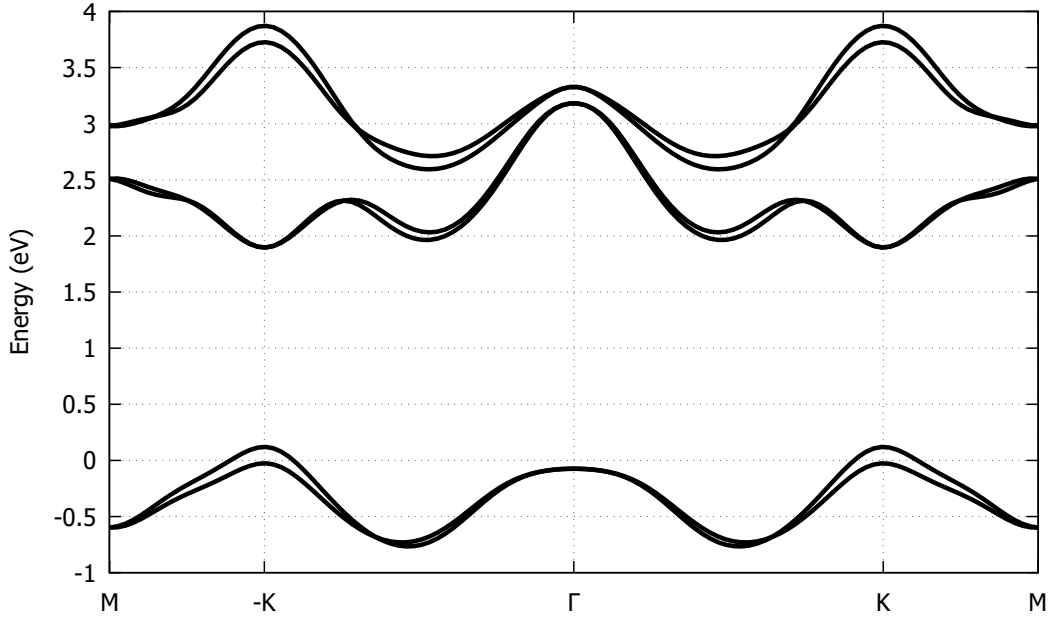


Figure 2: Band structure of monolayer-MoS<sub>2</sub> along  $M \rightarrow -K \rightarrow \Gamma \rightarrow K \rightarrow M$  direction, SOC causes huge splits in band-structure at K and  $-K$  points.

## 2.3 System Hamiltonian

### 2.3.1 First Quantization Hamiltonian

In the present of an external electromagnetic field, the Hamiltonian for an electron in the independent electron approximation takes the form:

$$H_{1e} = \frac{(\mathbf{p} + e\mathbf{A})^2}{2m} + V_0(\mathbf{r}) - e\phi, \quad (14)$$

in which,  $\mathbf{A}(\mathbf{r}, t)$  is vector potential and  $\phi(\mathbf{r}, t)$  is scalar potential. With  $\mathbf{p} = -i\hbar\nabla$ , we expand  $(\mathbf{p} + e\mathbf{A})^2 = \mathbf{p}^2 + 2e\mathbf{A}\mathbf{p} + ei\hbar\nabla(\mathbf{A}) + (e\mathbf{A})^2$ . We have  $\nabla \cdot (\mathbf{A}) = 0$  due to Coulomb gauge, so the (14) become

$$H_{1e} = H_{1e}^0 + \frac{e}{m}\mathbf{A} \cdot \mathbf{p} + \frac{e^2\mathbf{A}^2}{2m} - e\phi, \quad (15)$$

with  $H_{1e}^0$  is the stationary Hamiltonian of a single electron particle:

$$H_{1e}^0 = \frac{\mathbf{p}^2}{2m} + V_0(\mathbf{r}), \quad (16)$$

and the rest is the Light-matter interaction Hamiltonian  $H_{1e}^{e-L}$ :

$$H_{1e}^{e-L} = \frac{e}{m}\mathbf{A} \cdot \mathbf{p} - e\phi + \frac{e^2\mathbf{A}^2}{2m}. \quad (17)$$

When we choose gauge  $\phi = 0$ , the electromagnetic field's potential relation between  $\mathbf{A}$  and  $\phi$  becomes:

$$\mathbf{E} = -\nabla\phi - \frac{\partial\mathbf{A}}{\partial t} = -\frac{\partial\mathbf{A}}{\partial t}, \quad (18)$$

$$\mathbf{A}(\mathbf{r}, t) = -\int_{-\infty}^t dt' \mathbf{E}(\mathbf{r}, t'). \quad (19)$$

Substitute  $\phi = 0$  into (15),

$$H_{1e}^{VG} = H_{1e}^0 + \frac{e}{m}\mathbf{A} \cdot \mathbf{p} + \frac{e^2\mathbf{A}^2}{2m}. \quad (20)$$

Define the velocity operator  $\mathbf{v} = \frac{i}{\hbar}[H_{1e}, \mathbf{r}] = \frac{\mathbf{p} + e\mathbf{A}}{m}$ ,  $H_{1e}^{VG}$  will have the form

$$H_{1e}^{VG} = H_{1e}^0 + e\mathbf{A} \cdot \mathbf{v} - \frac{e^2\mathbf{A}^2}{2m}, \quad (21)$$

In velocity gauge, we have light-matter interaction (17) have the form:

$$H_{1e}^{e-L} = \frac{e}{m}\mathbf{A} \cdot \mathbf{p} + \frac{e^2\mathbf{A}^2}{2m}, \quad (22)$$

The electron-electron interaction between two electrons can be described by Coulomb interaction Hamiltonian:

$$H^{e-e}(\mathbf{r}_i, \mathbf{r}_j) = \frac{1}{4\pi\epsilon\epsilon_0} \frac{e^2}{|\mathbf{r}_i - \mathbf{r}_j|}, \quad (23)$$

in which the  $\epsilon_0$  is the vacuum permittivity,  $\epsilon$  is relative permittivity and  $\mathbf{r}$  is the distant between two electrons, all will be in SI unit. Combine (22), (23), and (16) to have Hamiltonian for the electron system in lattice interacting with the present of an external electromagnetic field:

$$H = \sum_i H_{1e}(\mathbf{r}_i, t) = \sum_i H_{1e}^0(\mathbf{r}_i) + \sum_i H_{1e}^{e-L}(\mathbf{r}_i, t) + \frac{1}{2} \sum_{\mathbf{r}_i, \mathbf{r}_j} H^{e-e}(\mathbf{r}_i, \mathbf{r}_j). \quad (24)$$

### 2.3.2 Second Quantization Hamiltonian

From (24), the second quantization Hamiltonian in Bloch basics  $\{|\psi_{\lambda\mathbf{k}}\rangle\}$  has the form:

$$\begin{aligned} H &= H^0 + H^{e-L} + H^{e-e}, \\ H^0 &= \sum_{\lambda\lambda'\mathbf{k}\mathbf{k}'} \langle\psi_{\lambda\mathbf{k}}| H_{1e}^0(\mathbf{r}) |\psi_{\lambda'\mathbf{k}'}\rangle c_{\lambda\mathbf{k}}^\dagger c_{\lambda'\mathbf{k}'}, \\ H^{e-L} &= \sum_{\lambda\lambda'\mathbf{k}\mathbf{k}'} \langle\psi_{\lambda\mathbf{k}}| H^{e-L}(\mathbf{r}) |\psi_{\lambda'\mathbf{k}'}\rangle c_{\lambda\mathbf{k}}^\dagger c_{\lambda'\mathbf{k}'}, \\ H^{e-e} &= \frac{1}{2} \sum_{\mathbf{k},\mathbf{k}',\mathbf{q}} \sum_{\alpha\beta\gamma\delta} W_{\mathbf{k},\mathbf{k}',\mathbf{q}}^{\alpha\beta\gamma\delta} c_{\alpha,\mathbf{k}+\mathbf{q}}^\dagger c_{\beta,\mathbf{k}'-\mathbf{q}}^\dagger c_{\gamma,\mathbf{k}} c_{\delta,\mathbf{k}'}, \end{aligned} \quad (25)$$

in which the basics is orthonormal:  $\langle\psi_{\lambda\mathbf{k}}|\psi_{\lambda'\mathbf{k}'}\rangle = 1$ , and the creation and annihilation operators satisfied the anti-commutate relation:

$$\{c_{\lambda,\mathbf{k}}, c_{\lambda',\mathbf{k}'}\} = \{c_{\lambda,\mathbf{k}}^\dagger, c_{\lambda',\mathbf{k}'}^\dagger\} = 0, \quad \{c_{\lambda,\mathbf{k}}, c_{\lambda',\mathbf{k}'}^\dagger\} = \delta_{\lambda,\lambda'}\delta_{\mathbf{k},\mathbf{k}'}. \quad (26)$$

If we choosing the basics is eigenvector of  $H_{1e}^0$  then  $H^0$  becomes:

$$H^0 = \sum_{\lambda\mathbf{k}} \varepsilon_\lambda(\mathbf{k}) c_{\lambda\mathbf{k}}^\dagger c_{\lambda\mathbf{k}}. \quad (27)$$

In VG, the elements of interaction Hamiltonian matrix  $\langle\psi_{\lambda\mathbf{k}}| H^{e-L}(\mathbf{r}, t) |\psi_{\lambda'\mathbf{k}'}\rangle$  is:

$$\begin{aligned} \langle\psi_{\lambda\mathbf{k}}| H^{e-L}(\mathbf{r}, t) |\psi_{\lambda'\mathbf{k}'}\rangle &= \langle\psi_{\lambda\mathbf{k}}| \frac{e}{m} \mathbf{A}(\mathbf{r}, t) \cdot \mathbf{p} |\psi_{\lambda'\mathbf{k}'}\rangle + \frac{e^2 A^2}{2m} \delta_{\lambda\lambda'} \delta_{\mathbf{k}\mathbf{k}'} \\ &\approx \frac{e}{m} \mathbf{A}(t) \cdot \langle\psi_{\lambda\mathbf{k}}| \mathbf{p} |\psi_{\lambda'\mathbf{k}'}\rangle + \frac{e^2 A^2}{2m} \delta_{\lambda\lambda'} \delta_{\mathbf{k}\mathbf{k}'}, \end{aligned} \quad (28)$$

where

$$\begin{aligned} \langle\psi_{\lambda\mathbf{k}}| \mathbf{p} |\psi_{\lambda'\mathbf{k}'}\rangle &= \int \frac{d^3r}{V} e^{-i\mathbf{k}\cdot\mathbf{r}} u_{\lambda\mathbf{k}}^*(\mathbf{r}) \hat{\mathbf{p}} (e^{i\mathbf{k}'\cdot\mathbf{r}} u_{\lambda'\mathbf{k}'}(\mathbf{r})) \\ &= \int \frac{d^3r}{V} e^{i(\mathbf{k}'-\mathbf{k})\cdot\mathbf{r}} u_{\lambda\mathbf{k}}^*(\mathbf{r}) (\hbar\mathbf{k} + \hat{\mathbf{p}}) u_{\lambda'\mathbf{k}'}(\mathbf{r}) \\ &= \frac{1}{N} \sum_i e^{i(\mathbf{k}'-\mathbf{k})\mathbf{R}_i} \int_{V_{Cell}} \frac{d^3r}{V_{Cell}} e^{i(\mathbf{k}'-\mathbf{k})\cdot\mathbf{r}} u_{\lambda\mathbf{k}}^*(\mathbf{r}) (\hbar\mathbf{k} + \hat{\mathbf{p}}) u_{\lambda'\mathbf{k}'}(\mathbf{r}). \end{aligned} \quad (29)$$

We include the Long-wavelength approximation  $\mathbf{k}', \mathbf{k} \ll \frac{2\pi}{a}$  to have:

$$\begin{aligned} (29) &\approx \frac{1}{N} \sum_i e^{i(\mathbf{k}'-\mathbf{k})\mathbf{R}_i} \int_{V_{Cell}} \frac{d^3r}{V_{Cell}} u_{\lambda\mathbf{k}}^*(\mathbf{r}) (\hbar\mathbf{k}' + \hat{\mathbf{p}}) u_{\lambda'\mathbf{k}'}(\mathbf{r}) \\ &\approx \frac{1}{N} \sum_i e^{i(\mathbf{k}'-\mathbf{k})\mathbf{R}_i} (\hbar\mathbf{k}' \langle u_{\lambda\mathbf{k}} | u_{\lambda'\mathbf{k}'} \rangle + \langle u_{\lambda\mathbf{k}} | \hat{\mathbf{p}} | u_{\lambda'\mathbf{k}'} \rangle), \end{aligned} \quad (30)$$

using relation  $\sum_i e^{i(\mathbf{k}'-\mathbf{k})\mathbf{R}_i} = N\delta_{\mathbf{k}',\mathbf{k}}$  for (30) to become

$$\langle\psi_{\lambda\mathbf{k}}| \mathbf{p} |\psi_{\lambda'\mathbf{k}'}\rangle \approx (\mathbf{p}_{\lambda\lambda'}(\mathbf{k}) + \hbar\mathbf{k}\delta_{\lambda\lambda'})\delta_{\mathbf{k},\mathbf{k}'}. \quad (31)$$

In which

$$\mathbf{p}_{\lambda\lambda'}(\mathbf{k}) = \langle u_{\lambda\mathbf{k}} | \mathbf{p} | u_{\lambda'\mathbf{k}} \rangle. \quad (32)$$

Define  $H_{1e}^0(\mathbf{k}) = e^{-i\mathbf{k}\mathbf{r}} H_{1e}^0 e^{i\mathbf{k}\mathbf{r}}$  and using the relation:  $[H_{1e}^0, \mathbf{r}] = -i\frac{\hbar}{m}\mathbf{p}$  to have

$$\mathbf{p}_{\lambda\lambda'}(\mathbf{k}) = \frac{m}{\hbar} \langle u_{\lambda\mathbf{k}} | \nabla_{\mathbf{k}} H_{1e}^0(\mathbf{k}) | u_{\lambda'\mathbf{k}} \rangle. \quad (33)$$

Therefore, the light-matter interaction part of the second quantization Hamiltonian has the following form:

$$H^{e-L} = \frac{e}{m} \mathbf{A}(t) \cdot \sum_{\lambda\lambda'\mathbf{k}} \mathbf{p}_{\lambda\lambda'}(\mathbf{k}) c_{\lambda\mathbf{k}}^\dagger c_{\lambda'\mathbf{k}} + \left( \hbar\mathbf{k} + \frac{e^2 \mathbf{A}^2}{2m} \right) \sum_{\lambda\mathbf{k}} c_{\lambda\mathbf{k}}^\dagger c_{\lambda\mathbf{k}}. \quad (34)$$

The  $H^{e-e}$  derivation will be presented in Appendix B. Thus, the many-body electron system Hamiltonian in second quantization in VG have the form:

$$\begin{aligned} H &= H_{1e}^0 + H^{e-e} + H^{e-L} \\ &= \sum_{\lambda\mathbf{k}} \varepsilon_{\mathbf{k}} c_{\lambda\mathbf{k}}^\dagger c_{\lambda\mathbf{k}} \\ &\quad + \frac{1}{2} \sum_{\mathbf{k}, \mathbf{k}', \mathbf{q}} \sum_{\alpha\beta\gamma\delta} W_{\mathbf{k}, \mathbf{k}', \mathbf{q}}^{\alpha\beta\gamma\delta} c_{\alpha, \mathbf{k}+\mathbf{q}}^\dagger c_{\beta, \mathbf{k}'-\mathbf{q}}^\dagger c_{\gamma, \mathbf{k}} c_{\delta, \mathbf{k}'} \\ &\quad + \frac{e}{m} \mathbf{A}(t) \cdot \sum_{\lambda\lambda'\mathbf{k}} \mathbf{p}_{\lambda\lambda'}(\mathbf{k}) c_{\lambda\mathbf{k}}^\dagger c_{\lambda'\mathbf{k}} + \left( \hbar\mathbf{k} + \frac{e^2 \mathbf{A}^2}{2m} \right) \sum_{\lambda\mathbf{k}} c_{\lambda\mathbf{k}}^\dagger c_{\lambda\mathbf{k}}, \end{aligned} \quad (35)$$

where the Coulomb interaction matrix elements are:

$$W_{\mathbf{k}, \mathbf{k}', \mathbf{q}}^{\alpha\beta\gamma\delta} = V_{ee}(\mathbf{q}) \langle u_{\alpha\mathbf{k}+\mathbf{q}} | u_{\delta\mathbf{k}} \rangle \langle u_{\beta\mathbf{k}'-\mathbf{q}} | u_{\gamma\mathbf{k}'} \rangle, \quad (36)$$

with the 2-D Coulomb interaction in momentum space:

$$V_{ee}(\mathbf{q}) = \frac{e^2}{2\varepsilon\varepsilon_0 L^2} \frac{1}{|\mathbf{q}|}. \quad (37)$$

## 2.4 Semiconductor Bloch Equation

With definition of density matrix elements,

$$\rho_{\lambda\lambda'}(\mathbf{k}) = \langle c_{\lambda'\mathbf{k}}^\dagger c_{\lambda\mathbf{k}} \rangle, \quad (38)$$

we using the motion equation in Heisenberg picture for operator  $c_{\lambda'\mathbf{k}}^\dagger c_{\lambda\mathbf{k}}$  and take expected value to have:

$$\frac{d}{dt} \langle c_{\lambda'\mathbf{k}}^\dagger c_{\lambda\mathbf{k}} \rangle = \frac{i}{\hbar} \langle [H, c_{\lambda'\mathbf{k}}^\dagger c_{\lambda\mathbf{k}}] \rangle. \quad (39)$$

Through the derivation in Appendix C, we have obtained the Semiconductor Bloch Equation(s) (SBE) with Coulomb interaction in the Hartree-Fock Approximation:

$$\begin{aligned} \frac{d}{dt} \rho_{\lambda\lambda'}(\mathbf{k}) &= -\frac{i}{\hbar} (\varepsilon_{\lambda}(\mathbf{k}) - \varepsilon_{\lambda'}(\mathbf{k})) \rho_{\lambda\lambda'}(\mathbf{k}) - \frac{ie}{\hbar m} \mathbf{A}(t) \sum_{\mu} [\mathbf{p}_{\lambda\mu}(\mathbf{k}) \rho_{\mu\lambda'}(\mathbf{k}) - \rho_{\lambda\mu}(\mathbf{k}) \mathbf{p}_{\mu\lambda'}(\mathbf{k})] \\ &\quad + \frac{i}{\hbar} [\Omega_{\lambda\mu}(\mathbf{k}) \rho_{\mu\lambda'}(\mathbf{k}) - \rho_{\lambda\mu}(\mathbf{k}) \Omega_{\mu\lambda'}(\mathbf{k})] + \frac{d}{dt} \rho_{\lambda\lambda'}(\mathbf{k}) \Big|_{\text{scat.}}. \end{aligned} \quad (40)$$

In which

$$\Omega_{\mu\nu}(\mathbf{k}) = \sum_{\alpha\beta\mathbf{q}} W_{\mathbf{k},\mathbf{k}+\mathbf{q},\mathbf{q}}^{\alpha\mu\beta\nu} \rho_{\alpha\beta}(\mathbf{k} + \mathbf{q}). \quad (41)$$

In (40) for the  $\rho_{\lambda\lambda}(\mathbf{k})$ , the density of electrons in the conduction bands and the hole densities in valence bands can be neglected due to the weak external electromagnetic field, which is also referred to as the "Low Excitation Limit". Therefore,

$$\left( \frac{d}{dt} \rho(\mathbf{k}) \Big|_{\text{scat.}} \right)_{\lambda\lambda} \rightarrow 0$$

The term "interband polarization" describes the decay of quantum coherence. A common and generally accurate approximation is to use the dephasing time parameter  $T_2$ , also known as the transverse relaxation time. This simple approximation is limited by nonlinear and non-Markovian effects, which, as mentioned earlier, can be ignored in this work. Therefore,

$$\left( \frac{d}{dt} \rho(\mathbf{k}) \Big|_{\text{scat.}} \right)_{\lambda\lambda'} \approx -\frac{\rho_{\lambda\lambda'}(\mathbf{k})}{T_2} \quad \forall \lambda \neq \lambda'. \quad (42)$$

Give us Semiconductor Bloch Equation<sup>20</sup> for numerical solving

$$\begin{aligned} \frac{d}{dt} \rho_{\lambda\lambda'}(\mathbf{k}) = & -\frac{i}{\hbar} (\varepsilon_{\lambda}(\mathbf{k}) - \varepsilon_{\lambda'}(\mathbf{k})) \rho_{\lambda\lambda'}(\mathbf{k}) - \frac{ie}{\hbar m} \mathbf{A}(t) \sum_{\mu} (\mathbf{p}_{\lambda\mu}(\mathbf{k}) \rho_{\mu\lambda'}(\mathbf{k}) - \rho_{\lambda\mu}(\mathbf{k}) \mathbf{p}_{\mu\lambda'}(\mathbf{k})) \\ & + \frac{i}{\hbar} (\Omega_{\lambda\mu}(\mathbf{k}) \rho_{\mu\lambda'}(\mathbf{k}) - \rho_{\lambda\mu}(\mathbf{k}) \Omega_{\mu\lambda'}(\mathbf{k})) - \frac{1}{T_2} \rho_{\lambda\lambda'}(\mathbf{k}) (1 - \delta_{\lambda\lambda'}), \end{aligned} \quad (43)$$

where

$$\Omega_{\mu\nu}(\mathbf{k}) = \sum_{\alpha\beta\mathbf{q}} W_{\mathbf{k},\mathbf{k}+\mathbf{q},\mathbf{q}}^{\alpha\mu\beta\nu} \rho_{\alpha\beta}(\mathbf{k} + \mathbf{q}) \quad (44)$$

## 2.5 Polarization Density

Polarization density is calculated from the trace of dipole and density matrix multiplication

$$\mathbf{P}(t) = \frac{e}{L^2} \sum_{\mathbf{k}} \text{Tr} [\vec{\xi}(\mathbf{k}) \rho(\mathbf{k}, t)] = \frac{e}{L^2} \sum_{\lambda\lambda'\mathbf{k}} \vec{\xi}_{\lambda\lambda'}(\mathbf{k}) \rho_{\lambda'\lambda}(\mathbf{k}, t). \quad (45)$$

Take the sum over all  $\mathbf{k}$ -points in the first BZ in 2D  $\mathbf{k}$ -grid through the integral

$$\sum_{\mathbf{k}} \dots \rightarrow \frac{L^2}{(2\pi)^2} \int_{\text{BZ}} d^2k \dots \quad (46)$$

Include it into polarization density (45) to have:

$$\mathbf{P}(t) = \frac{e}{L^2} \sum_{\mathbf{k}} \text{Tr} [\vec{\xi}(\mathbf{k}) \rho(\mathbf{k}, t)] = \frac{1}{(2\pi)^2} \sum_{\lambda\lambda'} \int \vec{\xi}_{\lambda\lambda'}(\mathbf{k}) \rho_{\lambda'\lambda}(\mathbf{k}, t) d\mathbf{k}, \quad (47)$$

in which the dipole  $\vec{\xi}_{\lambda\lambda'}(\mathbf{k})$  can be calculated through  $\vec{p}_{\lambda\lambda'}(\mathbf{k})$  as derived in appendix D:

$$\vec{\xi}_{\lambda\lambda'}(\mathbf{k}) = -\frac{i\hbar}{m} \frac{\vec{p}_{\lambda\lambda'}(\mathbf{k})}{\varepsilon_{\lambda}(\mathbf{k}) - \varepsilon_{\lambda'}(\mathbf{k})}. \quad (48)$$

The Numerical result will be taken by using the Riemann Sum Integral.



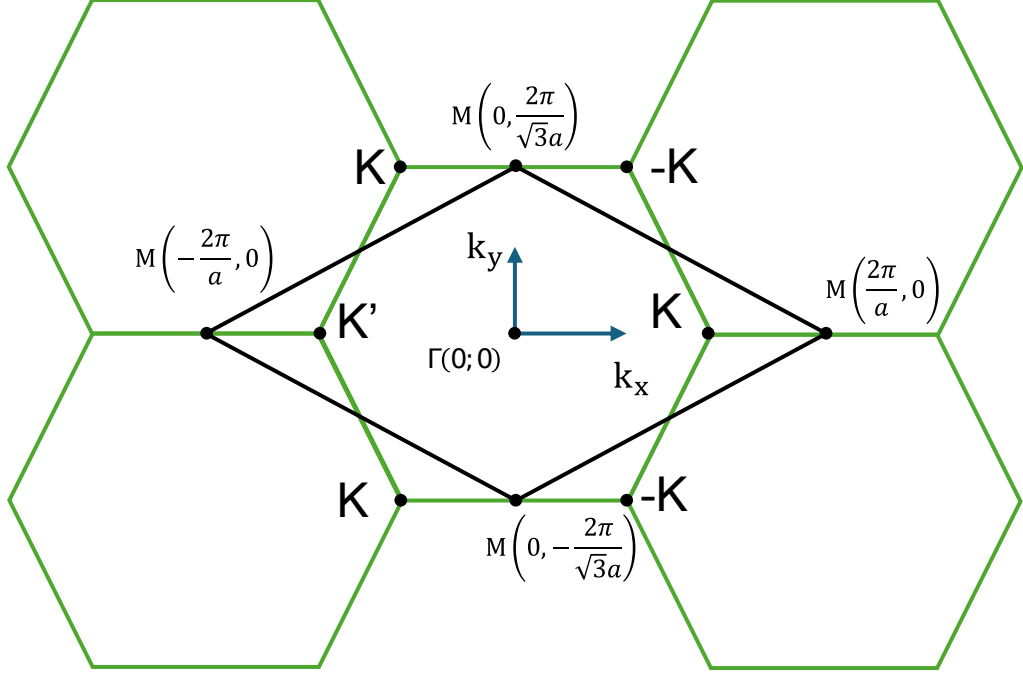


Figure 3: Rhombus primitive unit cell construct through four M-Points, it have the same Area as first the Brillouin zone (the green Hexagon bounded with "K-point" and "K'-point")

### 3 Numerical Methods

#### 3.1 Numerical Sum Over k-Space

Monolayer TMD's actual lattice, denoted as  $MX_2$ , possesses the  $D3h$  point-group symmetry, as illustrated in (Figure 1). The 2D first Brillouin zone takes on the shape of a hexagon. This study concentrates on the linear abortion spectrum, a feature that relies heavily on the k-points with the direct band gap of this material. To numerical calculate the eq. (47), we need to take numerical integral over the first BZ, which is inconvenient when working with the hexagon shape. Furthermore, a direct band gap is observed at the K and K' points in the first BZ, as depicted in fig. (2). There are three K and three K' points situated at the edge of the first BZ as shown in fig. 3, with each points being shared between three BZ. Consequently, we need to calculate the average numerical position by adding up the positions and then dividing by the number of points, which can pose further challenges for the many-body problems we are addressing.

To address this, we introduce the use of the rhombus primitive cell, as shown in Figure 3. This cell is constructed from 4 M-points located between K and K' on the edge of the hexagon, enabling us to focus on the properties of K and K' points both individually and in pairs.

In order to establish a new coordinate system, we will utilize the two unit vectors located at the left corner of the rhombus  $u_1, u_2$  as shown in fig. 4, which will be reference to as the "Rhombus basics" hereinafter. To change coordinate of a point which has coordinate  $(v_1, v_2)$  in Rhombus basics into coordinate  $(x, y)$  in Cartesian Oxy basics and vice versa, we will use the transformation matrix:

$$\begin{pmatrix} x \\ y \end{pmatrix} = \frac{2\pi}{a} \left[ \begin{pmatrix} 1 & 1 \\ \frac{1}{\sqrt{3}} & -\frac{1}{\sqrt{3}} \end{pmatrix} \begin{pmatrix} v_1 \\ v_2 \end{pmatrix} - \begin{pmatrix} 1 \\ 0 \end{pmatrix} \right] \quad (49)$$

Since the coordinate system  $Ou_1u_2$  is a continuous variable, we need to convert it into discrete coordinates in order to proceed with a numerical solution. To do this, we divide the vectors  $u_1$  and

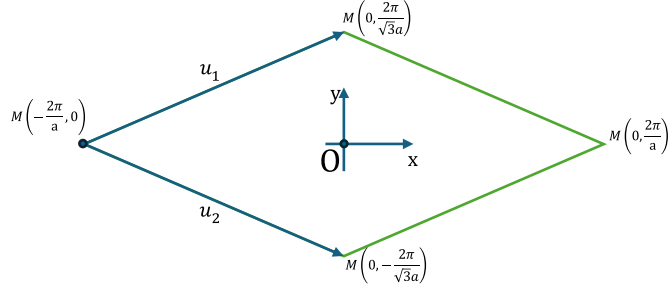


Figure 4: New Basics Based on the rhombus unit vectors

$u_2$  into  $nk$  equal segments, which are then labeled as  $nk_1$  and  $nk_2$ , respectively.

For a point label as  $(nk_1, nk_2)$  in discrete coordinate, its coordinate in Cartesian basics  $(x, y)$  can be obtain by:

$$\begin{pmatrix} x \\ y \end{pmatrix} = \frac{2\pi}{n_k a} \begin{pmatrix} 1 & 1 \\ \frac{1}{\sqrt{3}} & -\frac{1}{\sqrt{3}} \end{pmatrix} \begin{pmatrix} nk_1 \\ nk_2 \end{pmatrix} - \frac{2\pi}{a} \begin{pmatrix} 1 \\ 0 \end{pmatrix} \quad (50)$$

### 3.2 Cut Off K-point Technique

In our research, we are focusing on the transition between the valence and conduction bands around the K and K' points. We achieve this by using a small intensity electric field and limiting the photon energy to extract the band gap  $E_{gap}$ . However, the calculation of the Coulomb interaction for every point in the Rhombus with other points all over the Rhombus is not efficient in terms of time cost and convergence. As demonstrated in the 2-D Coulomb interaction equation (37), the Coulomb potential is inversely proportional to the distance between two points in k-space. To address this issue, we are introducing a technique to limit the points taken into account in the Coulomb interaction part.

In the diagram shown in figure 5, a circle is drawn around the K' point with a radius of  $k_{cut}$ .

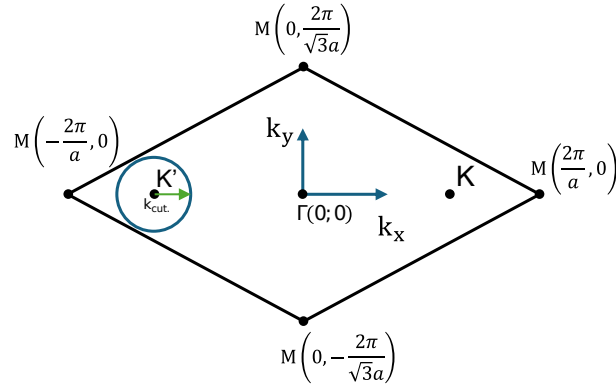


Figure 5: k-radius show the cutoff circle around K' points

When calculating the equation (43) at a k-point, if this k-point is outside the circle, we use

$$\Omega_{\mu\nu}(\mathbf{k}) = 0 \quad \forall \mu, \nu.$$

However, if the k-point is inside the circle, we will only consider interactions with other points that are also inside the circle.

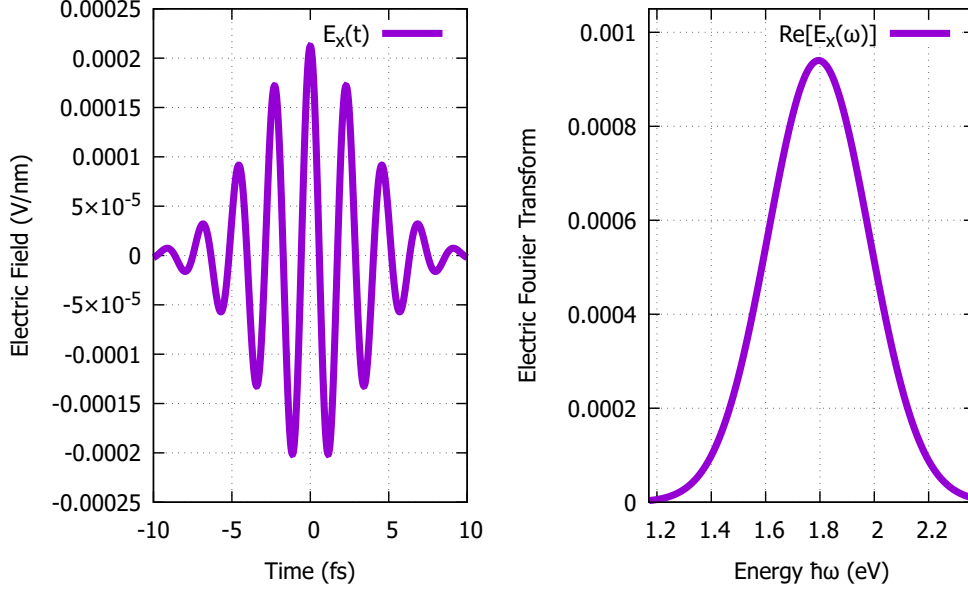


Figure 6: Electric field on Ox direction and it Fourier Transform

In summary, we approximate the Coulomb interaction matrix elements:

$$W_{\mathbf{k},\mathbf{k}',\mathbf{q}}^{\alpha\mu\beta\nu} \approx W_{\mathbf{k},\mathbf{k}',\mathbf{q}}^{\alpha\mu\beta\nu} \theta(k_{cut.} - |\mathbf{k} - \mathbf{k}_{K'}|) \theta(k_{cut.} - |\mathbf{k}' - \mathbf{k}_{K'}|).$$

Where  $\theta(k)$  is the Heaviside function, the Coulomb interaction is excluded if either point is inside the circle. The same process applies for the K point.

### 3.3 Numerical Analyzing

The linear absorption spectrum is determined by<sup>20</sup>

$$\alpha(\omega) \propto \text{Im} \left\{ \frac{P(\omega)}{E(\omega)} \right\}. \quad (51)$$

In which  $\mathbf{P}(\omega) = \int_{-\infty}^{\infty} \mathbf{P}(t) e^{i\omega t} dt$  and  $\mathbf{E}(\omega) = \int_{-\infty}^{\infty} \mathbf{E}(t) e^{i\omega t} dt$  is Fourier transform for polarization density and Electric field. This integral can be approximated using a Riemann sum with the cutoff point by using condition  $\mathbf{E}(t_{cutoff}) \lesssim 10^{-6} |\max \mathbf{E}(t)|$  and  $\mathbf{P}(t_{cutoff}) \lesssim 10^{-6} |\max \mathbf{P}(t)|$ . In this work, we are using the electric field in form of Gaussian wave:

$$\mathbf{E}(t) = E_0 e^{-\frac{t^2}{\tau_L^2}} (\cos(\omega_0 t), 0), \quad (52)$$

with the  $E_0$  is the maximal amplitude, so  $\hbar\omega_0 = E_{\text{gap}}$ ,  $\tau_L$  is the duration of the Gaussian pulse, and  $t$  is time, all will be calculated in SI units. The  $E_x(t)$  and it Fourier transform shape shown in fig. 6.

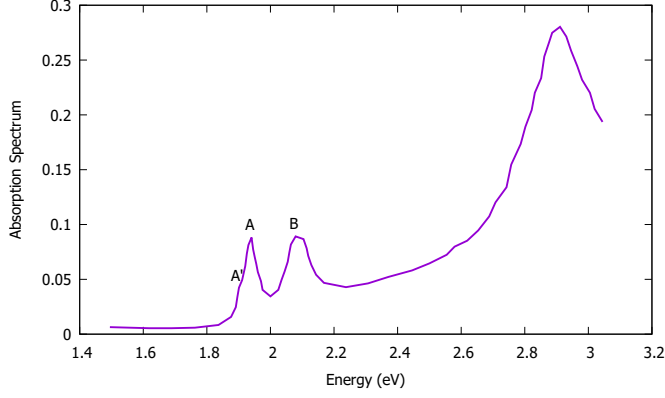


Figure 7: Measure Absorption Spectrum of MoS<sub>2</sub> at  $T = 5K$  extracted from<sup>7</sup>, two Exciton resonances labeled by A and B, and small trion peak labeled with A'.

$\varepsilon$	1.0	1.5	2.0	2.5
$E_{\text{bind.}}(eV)$	-0.95	-0.55	-0.36	-0.25

Table 2: Exciton binding energy with difference dielectric  $\varepsilon$

## 4 Results and Discussion

In a previous study<sup>7</sup>, the absorption spectrum of MoS<sub>2</sub> at  $T = 5K$  was measured and presented in figure 7. The results revealed two exciton resonances labeled as A and B, which were observed at energy levels of 1.9 and 2.1 eV, respectively. Additionally, a small trion peak was observed before the A peak. The splitting between the exciton and trion absorption peaks was approximately 34 meV at 5K.

When solving the semiconductor Bloch equations (SBE) numerically, we utilize the external electric field as follows:  $E_0 = \frac{3}{\sqrt{2}} \times 10^3 \text{ V/cm}$ ,  $\hbar\omega_0 = E_{\text{gap}} = 1.77 \text{ eV}$ , time step  $\Delta t = 0.02 \text{ fs}$ ,  $= 20(f s^{-1})$ , and cutoff the Coulomb interaction at  $3.0 \text{ nm}^{-1}$  around K and K' points to simplify the calculation. By simulating with the given parameters, we observe that the density of electrons in the conduction band after the external field passes is relatively small compared to the initial electron density in the valence band ( $1.10^7 \text{ cm}^{-2} \ll 1.10^{11} \text{ cm}^{-2}$ ), which confirms our discussion on the neglect of electron-electron scattering in equation (43). We perform Fourier transforms of energies from above and below the band gap by 1 eV. There are three main parameters we can adjust to obtain results that agree with or predict recent or future measurements: dielectric  $\varepsilon$ ,  $T_2$  parameter, and the number of k points on the k grid.

In Figure 8, our results for calculating the Absorption Spectrum with LDA parameters are presented, where the dielectric constant is  $\varepsilon = 2.5$  and the difference dephasing parameter is  $T_2$ . As  $T_2$  increases, two main peaks become clearer at 1.528 and 1.640 eV, indicating a binding energy of approximately 0.25 eV.

We present our results for calculating the Absorption Spectrum using the LDA parameter and the difference dielectric  $\varepsilon$  in Figure 9. As the dielectric constant  $\varepsilon$  increases, two main peaks shift to the left, which can be used to determine the fitting value with the experiment, the exciton binding energy result vary on dielectric parameter  $\varepsilon$  shown in table 2.

In Figure 10, we present our calculated results with varying numbers of k-grid points, using a dielectric constant of  $\varepsilon = 2.5$  to demonstrate the convergence of the results. The calculations converge

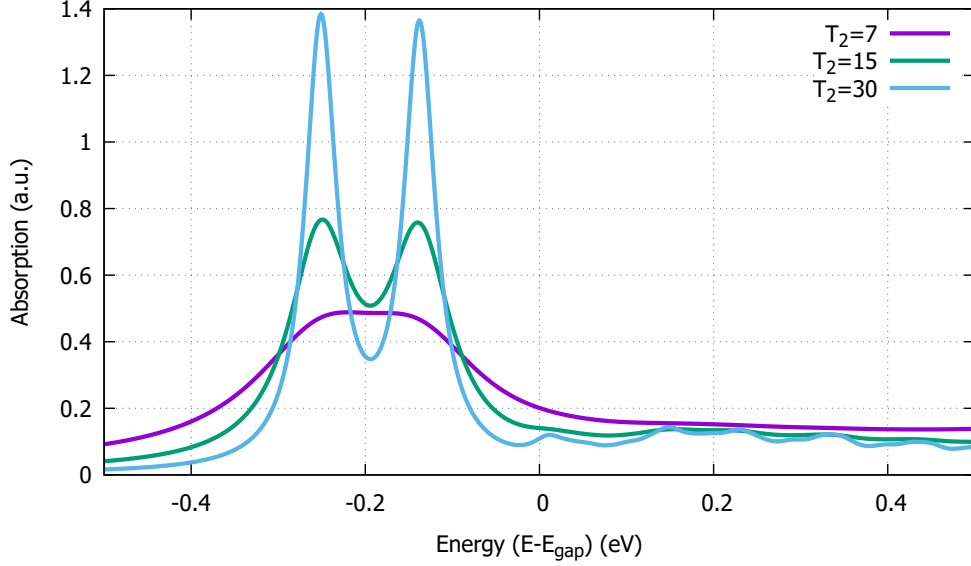


Figure 8: Absorption Spectrum with difference  $T_2$

when the value of  $nk$  is between 60 and 120. To strike a balance between precision and time cost, we opt for  $nk = 60$  for the subsequent calculations.

With a small  $T_2$  of 15 (fs), the results in 8 have already shown two main exciton peaks in comparison with the experimental results in 7. However, as the  $T_2$  increases at the cost of simulation time, we can see smaller exciton peaks in the absorption spectrum, as described in fig. 8. These A and B exciton resonances involve the conduction band and two valence bands (split due to spin-orbit coupling) near the K and  $-K$  points, as shown in the band structure in fig. 2, providing evidence for the good approximation of the transverse relaxation time  $T_2$ . In our results shown in Fig. 8 and the experiment by Zhang et al.<sup>7</sup> in Fig. 7, we observed that the energy peak does not align with the expected value for the dielectric constant  $\epsilon = 2.5$ . As per the data in Fig. 7<sup>7</sup>, the exciton peaks are situated at 1.9 and 2.1 eV, while in our calculations, the two peaks are at 1.528 and 1.640 eV, indicating a binding energy of the exciton of about 0.25 eV. If we only consider the distance from the band gap, our result is smaller than some previous calculations predicting the binding energy between 0.5 eV to 1 eV<sup>8–11</sup>. This result agrees with more precise calculations and measurements<sup>6;7;21</sup>. The difference in band gap energy can be attributed to the use of DFT calculations in our model<sup>14</sup>. This model does not consider the band gap shift caused by the underlying layers and temperature variations in the experimental measurement. The absence of the trion peak in Figure 1 is due to the trion involving an interaction between three particles (2 holes and 1 electron for a positive trion, 1 hole and 2 electrons for a negative trion), which is not included in the Hartree-Fock approximation. To observe the trion peak, it is suggested to go beyond the HFA in established equations.

This model is effective and has advantages for calculation over BZ, but it also has disadvantages and requires denser  $k$ -grids for results to converge (as shown in Fig. 10) compared to DFT models or parabola approximation models. The Bare Coulomb interaction works well in calculating the linear absorption spectrum, but for a more realistic case, the shield Coulomb interaction must be taken into account<sup>22;23</sup>. The parameter  $T_2$  is proved to be a good approximation without requiring further techniques.

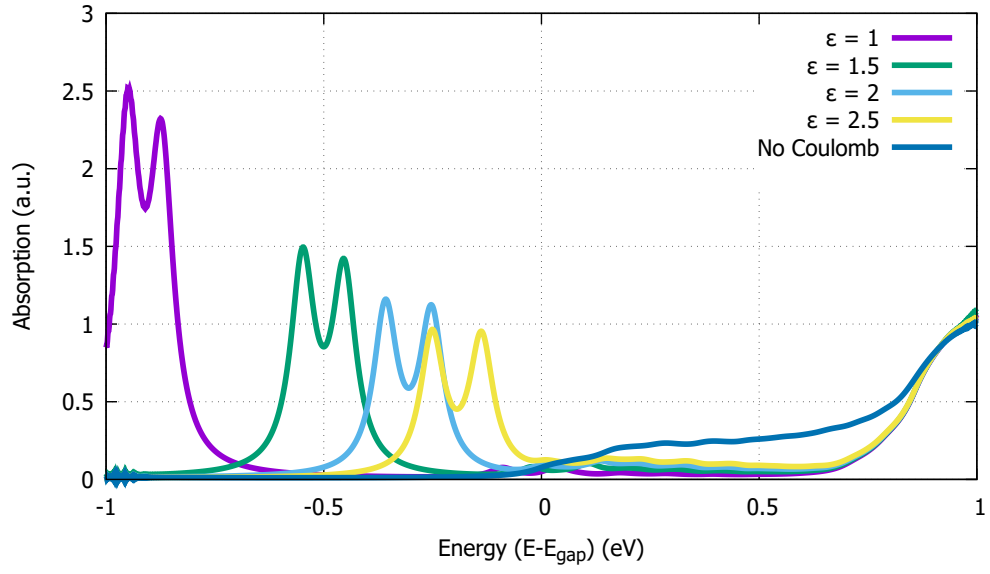


Figure 9: Absorption Spectrum with difference dielectric  $\epsilon$  and without Coulomb interaction

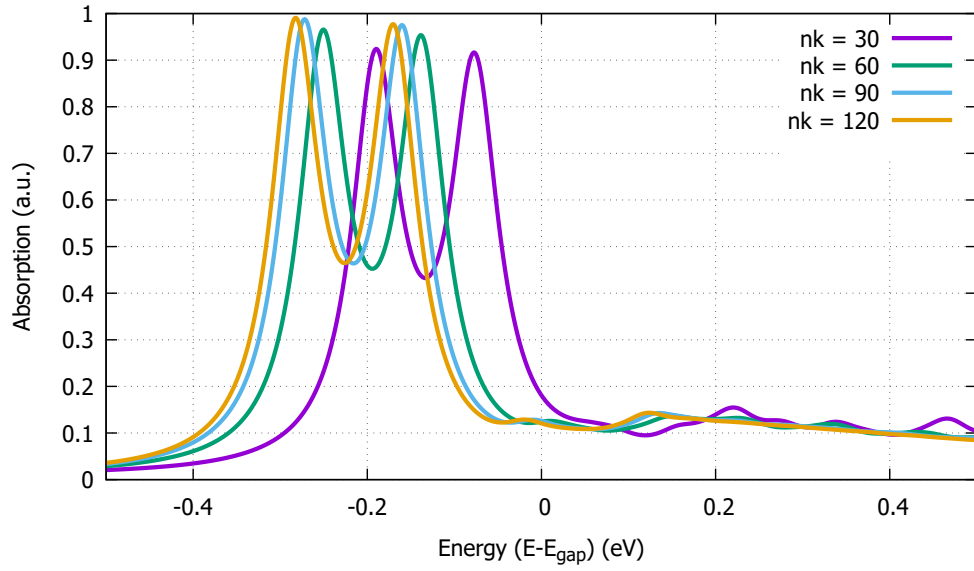


Figure 10: Absorption Spectrum with difference number of k-points

## 5 Conclusion and Further

In our research, we calculated the linear absorption of monolayer MoS<sub>2</sub> using a Tight-Binding three-band model with spin orbit coupling through semiconductor Bloch equations in Hartree-Fock approximation. We varied various parameters to analyze their relationship with the absorption spectrum and found that the results align with other calculations, indicating a significant binding energy up to two magnitude in comparison with other bulk semiconductors.

We did encounter some limitations, like the time-consuming process of enhancing the k-grid for better convergence and the discrepancy in the bandgap position as compared to experimental data. We also observed that the bare Coulomb interaction might not be adequate for an accurate depiction and should be fine-tuned for better outcomes.

For further researches, we can utilize this three-band tight-binding model to calculate other optoelectronic phenomena affected by excitons, such as high harmonic generation (HHG), high-order sideband generation (HSG), and photovoltaic current. When calculating the photovoltaic effect, it's important to consider the influence of Coulomb interactions. Without the consideration of Coulomb interactions, only the shift current is apparent, as we've calculated the current tensors as per ref. [24](#). However, once we include the Coulomb interaction, the ballistic current becomes significant, and the shift tensor current is also affected. It's crucial to account for Coulomb interactions to obtain a realistic picture of the photovoltaic effect.

## References

- [1] A. K. Geim and I. V. Grigorieva, “Van der Waals heterostructures,” *Nature*, vol. 499, pp. 419–425, July 2013. Publisher: Nature Publishing Group.
- [2] Q. H. Wang, K. Kalantar-Zadeh, A. Kis, J. N. Coleman, and M. S. Strano, “Electronics and optoelectronics of two-dimensional transition metal dichalcogenides,” *Nature Nanotechnology*, vol. 7, pp. 699–712, Nov. 2012.
- [3] J. Jiang, Z. Chen, Y. Hu, Y. Xiang, L. Zhang, Y. Wang, G.-C. Wang, and J. Shi, “Flexo-photovoltaic effect in MoS<sub>2</sub>,” *Nature Nanotechnology*, vol. 16, pp. 894–901, Aug. 2021. Publisher: Nature Publishing Group.
- [4] D. Xiao, W. Yao, and Q. Niu, “Valley-Contrasting Physics in Graphene: Magnetic Moment and Topological Transport,” *Physical Review Letters*, vol. 99, p. 236809, Dec. 2007. Publisher: American Physical Society.
- [5] W. Yao, D. Xiao, and Q. Niu, “Valley-dependent optoelectronics from inversion symmetry breaking,” *Physical Review B*, vol. 77, p. 235406, June 2008. Publisher: American Physical Society.
- [6] E. V. Kirichenko and V. A. Stephanovich, “The influence of Coulomb interaction screening on the excitons in disordered two-dimensional insulators,” *Scientific Reports*, vol. 11, p. 11956, June 2021. Number: 1 Publisher: Nature Publishing Group.
- [7] C. Zhang, H. Wang, W. Chan, C. Manolatou, and F. Rana, “Absorption of light by excitons and trions in monolayers of metal dichalcogenide  $\mathrm{MoS}_2$ : Experiments and theory,” *Physical Review B*, vol. 89, p. 205436, May 2014. Publisher: American Physical Society.
- [8] A. Ramasubramaniam, “Large excitonic effects in monolayers of molybdenum and tungsten dichalcogenides,” *Physical Review B*, vol. 86, p. 115409, Sept. 2012. Publisher: American Physical Society.
- [9] D. Y. Qiu, F. H. da Jornada, and S. G. Louie, “Optical Spectrum of  $\mathrm{MoS}_2$ : Many-Body Effects and Diversity of Exciton States,” *Physical Review Letters*, vol. 111, p. 216805, Nov. 2013. Publisher: American Physical Society.
- [10] T. Cheiwchanchamnangij and W. R. L. Lambrecht, “Quasiparticle band structure calculation of monolayer, bilayer, and bulk  $\mathrm{MoS}_2$ ,” *Physical Review B*, vol. 85, p. 205302, May 2012. Publisher: American Physical Society.
- [11] H. Shi, H. Pan, Y.-W. Zhang, and B. I. Yakobson, “Quasiparticle band structures and optical properties of strained monolayer  $\mathrm{MoS}_2$  and  $\mathrm{WS}_2$ ,” *Physical Review B*, vol. 87, p. 155304, Apr. 2013. Publisher: American Physical Society.
- [12] L. Meckbach, J. Hader, U. Huttner, J. Neuhaus, J. T. Steiner, T. Stroucken, J. V. Moloney, and S. W. Koch, “Ultrafast band-gap renormalization and build-up of optical gain in monolayer  $\mathrm{MoTe}_2$ ,” *Physical Review B*, vol. 101, p. 075401, Feb. 2020.
- [13] T. C. Berkelbach, M. S. Hybertsen, and D. R. Reichman, “Theory of neutral and charged excitons in monolayer transition metal dichalcogenides,” *Physical Review B*, vol. 88, p. 045318, July 2013.



- [14] G.-B. Liu, W.-Y. Shan, Y. Yao, W. Yao, and D. Xiao, “Three-band tight-binding model for monolayers of group-VIB transition metal dichalcogenides,” *Physical Review B*, vol. 88, p. 085433, Aug. 2013. Publisher: American Physical Society.
- [15] D. Xiao, G.-B. Liu, W. Feng, X. Xu, and W. Yao, “Coupled Spin and Valley Physics in Monolayers of  $\{\mathrm{MoS}\}_2$  and Other Group-VI Dichalcogenides,” *Physical Review Letters*, vol. 108, p. 196802, May 2012. Publisher: American Physical Society.
- [16] L. F. Mattheiss, “Band Structures of Transition-Metal-Dichalcogenide Layer Compounds,” *Physical Review B*, vol. 8, pp. 3719–3740, Oct. 1973. Publisher: American Physical Society.
- [17] S. Lebegue and O. Eriksson, “Electronic structure of two-dimensional crystals from ab initio theory,” *Physical Review B*, vol. 79, p. 115409, Mar. 2009. Publisher: American Physical Society.
- [18] Z. Y. Zhu, Y. C. Cheng, and U. Schwingenschlögl, “Giant spin-orbit-induced spin splitting in two-dimensional transition-metal dichalcogenide semiconductors,” *Physical Review B*, vol. 84, p. 153402, Oct. 2011. Publisher: American Physical Society.
- [19] C. Ataca, H. Şahin, and S. Ciraci, “Stable, Single-Layer MX<sub>2</sub> Transition-Metal Oxides and Dichalcogenides in a Honeycomb-Like Structure,” *The Journal of Physical Chemistry C*, vol. 116, pp. 8983–8999, Apr. 2012. Publisher: American Chemical Society.
- [20] H. Haug and S. W. Koch, *Quantum Theory Of The Optical And Electronic Properties Of Semiconductors (5th Edition)*. World Scientific Publishing Company, Jan. 2009. Google-Books-ID: 1J1IDQAAQBAJ.
- [21] C. Zhang, A. Johnson, C.-L. Hsu, L.-J. Li, and C.-K. Shih, “Direct Imaging of Band Profile in Single Layer MoS<sub>2</sub> on Graphite: Quasiparticle Energy Gap, Metallic Edge States, and Edge Band Bending,” *Nano Letters*, vol. 14, pp. 2443–2447, May 2014. Publisher: American Chemical Society.
- [22] D. Erben, A. Steinhoff, C. Gies, G. Schönhoff, T. O. Wehling, and F. Jahnke, “Excitation-induced transition to indirect band gaps in atomically thin transition-metal dichalcogenide semiconductors,” *Physical Review B*, vol. 98, p. 035434, July 2018.
- [23] D. Erben, A. Steinhoff, M. Lorke, and F. Jahnke, “Optical nonlinearities in the excited carrier density of atomically thin transition metal dichalcogenides,” *Physical Review B*, vol. 106, p. 045409, July 2022.
- [24] C. D. P. Vo and T. D. Huynh, “Calculation of shift current tensors in two-dimensional transition metal dichalcogenides,” *E3S Web of Conferences*, vol. 496, p. 02002, 2024. Publisher: EDP Sciences.

# Appendices

## A Electromagnetic Field - Charge Interaction Hamiltonian

From classical Electromagnetic Interaction, we derive the Interaction Hamiltonian between an electric charge and a classical/semi-classical electromagnetic field. The Coulomb's force and Lorentz's force for an electric charge in an electromagnetic field have the following form:

$$\vec{F} = q(\vec{E} + \vec{v} \times \vec{B}). \quad (53)$$

From Euler-Largrange equation, we have

$$\vec{F} = -\vec{\nabla}U + \frac{d}{dt}\left(\frac{\partial U}{\partial \vec{v}}\right), \quad (54)$$

To satisfied (54),  $U$  must be

$$U = q(\phi - \vec{v} \cdot \vec{A}). \quad (55)$$

From it, we can construct the Largrangian of the Interaction between the electric charge and classical Electromagnetic field

$$L = T - U = \frac{1}{2}m\vec{v}^2 + q\vec{v} \cdot \vec{A} - q\phi. \quad (56)$$

Canonical momentum for the charge is

$$\vec{p} = \frac{\partial L}{\partial \vec{v}} = m\vec{v} + q\vec{A}. \quad (57)$$

From that, we can construct classical Hamiltonian for electric charge in electromagnetic field

$$H = \vec{p} \cdot \vec{v} - L = \frac{1}{2m}(\vec{p} - q\vec{A})^2 + q\phi. \quad (58)$$

To quantization Hamiltonian, we change the classical position and canonical momentum to position and canonical momentum operators, respectively

$$\vec{p} \longrightarrow \hat{p}, \quad \vec{r} \longrightarrow \hat{r},$$

include this into (58) to get Hamiltonian operator:

$$\hat{H} = \frac{1}{2m}(\hat{p} - q\vec{A})^2 + q\phi \quad (59)$$

To confirm the Gauge variant of Schrödinger equation, we can start from it

$$i\hbar \frac{\partial}{\partial t} \psi = \hat{H} \psi = \left[ \frac{1}{2m}(\hat{p} - q\vec{A})^2 + q\phi \right] \psi. \quad (60)$$

Doing Gauge transform for the electromagnetic field and phase transform for the wave function

$$\vec{A} \longrightarrow \vec{A} - \vec{\nabla}\chi, \quad \phi \longrightarrow \phi + \frac{\partial \chi}{\partial t}, \quad \psi \longrightarrow e^{-i\frac{q}{\hbar}\chi} \psi,$$

include it into (60) to get

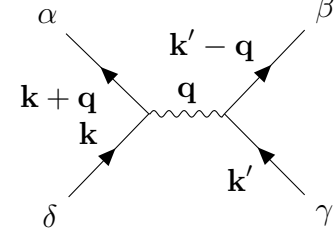
$$i\hbar \frac{\partial}{\partial t} e^{-i\frac{q}{\hbar}\chi} \psi = \left[ \frac{1}{2m}(\hat{p} - q(\vec{A} - \vec{\nabla}\chi))^2 + q(\phi + \frac{\partial \chi}{\partial t}) \right] e^{-i\frac{q}{\hbar}\chi} \psi.$$

## B Electron - Electron Interaction Hamiltonian

In this section, we will derive Hamiltonian for charge system in second quantization. Starting from Hamiltonian

$$H = \sum_{\mathbf{k}} \varepsilon_{\mathbf{k}} c_{\mathbf{k}}^{\dagger} c_{\mathbf{k}} + \frac{1}{2} \sum_{\mathbf{k}, \mathbf{k}', \mathbf{q}} \sum_{\alpha \beta \gamma \delta} W_{\mathbf{k}, \mathbf{k}', \mathbf{q}}^{\alpha \beta \gamma \delta} c_{\alpha, \mathbf{k} + \mathbf{q}}^{\dagger} c_{\beta, \mathbf{k}' - \mathbf{q}}^{\dagger} c_{\gamma, \mathbf{k}} c_{\delta, \mathbf{k}'} \quad (61)$$

the Coulomb matrix elements is



$$W_{\mathbf{k}, \mathbf{k}', \mathbf{q}}^{\alpha \beta \gamma \delta} = \langle \psi_{\alpha \mathbf{k} + \mathbf{q}} \psi_{\beta \mathbf{k}' - \mathbf{q}} | V_{ee} | \psi_{\gamma \mathbf{k}'} \psi_{\delta \mathbf{k}} \rangle =$$

$$= \int \frac{d^3 r}{V} \int \frac{d^3 r'}{V} e^{-i \mathbf{q}(\mathbf{r} - \mathbf{r}')} u_{\alpha \mathbf{k} + \mathbf{q}}^*(\mathbf{r}) u_{\beta \mathbf{k}' - \mathbf{q}}^*(\mathbf{r}') V_{ee}(\mathbf{r} - \mathbf{r}') u_{\gamma \mathbf{k}'}(\mathbf{r}') u_{\delta \mathbf{k}}(\mathbf{r}), \quad (62)$$

with

$$W_{ee}(\mathbf{r}) = \frac{e^2}{4\pi \varepsilon \varepsilon_0} \frac{1}{|\mathbf{r}|}, \quad (63)$$

we expand it using Fourier transform

$$\begin{aligned} W_{ee}(\mathbf{q}) &= \int \frac{d^3 \mathbf{r}}{V} W_{ee}(\mathbf{r}) e^{-i \mathbf{q} \cdot \mathbf{r}} = \frac{e^2}{4\pi \varepsilon \varepsilon_0 V} \int d^3 \mathbf{r} \frac{1}{|\mathbf{r}|} e^{-i \mathbf{q} \cdot \mathbf{r}} \\ &= \frac{e^2}{4\pi \varepsilon \varepsilon_0 V} \int_0^\infty \int_0^{2\pi} \int_{-\pi}^\pi \frac{1}{r} r^2 e^{-i q r \cos(\theta)} dr d\varphi \cos(\theta) d\theta \\ &= \frac{e^2}{2\varepsilon \varepsilon_0 V} \int_0^\infty \int_{-1}^1 r dr d\cos \theta e^{i q r \cos \theta} = -\frac{i}{q} \frac{e^2}{2\varepsilon \varepsilon_0 V} \int_0^\infty dr (e^{i q r} - e^{-i q r}) \\ &= -\frac{i}{q} \frac{e^2}{2\varepsilon \varepsilon_0 V} \lim_{\gamma \rightarrow 0} \int_0^\infty dr (e^{i q r} - e^{-i q r}) e^{-\gamma r} \\ &= \frac{e^2}{2\varepsilon \varepsilon_0 V} \lim_{\gamma \rightarrow 0} \left( \int_0^\infty \frac{e^{(i q - \gamma) r}}{i q - \gamma} dr - \int_0^\infty \frac{e^{-(i q + \gamma) r}}{i q + \gamma} dr \right) = \frac{e^2}{\varepsilon \varepsilon_0 V} \frac{1}{q^2}. \end{aligned} \quad (64)$$

Include (64) into (62) through reverse Fourier transform

$$\begin{aligned} W_{ee}(\mathbf{r}) &= \sum_{\mathbf{q}} W_{ee}(\mathbf{q}) e^{i \mathbf{q} \cdot \mathbf{r}} = \sum_{\mathbf{q}_{\parallel}, \mathbf{q}_{\perp}} \frac{e^2}{\varepsilon \varepsilon_0 V} \frac{1}{\mathbf{q}_{\parallel}^2 + q_{\perp}^2} e^{i \mathbf{q}_{\parallel} \mathbf{r}_{\parallel}} e^{i q_{\perp} \mathbf{r}_{\perp}} \\ &= \sum_{\mathbf{q}_{\parallel}} \frac{1}{2\pi/L_z} \frac{e^2}{\varepsilon \varepsilon_0 V} e^{i \mathbf{q}_{\parallel} \mathbf{r}_{\parallel}} \int dq_{\perp} \frac{e^{i q_{\perp} \mathbf{r}_{\perp}}}{\mathbf{q}_{\parallel}^2 + q_{\perp}^2}, \end{aligned} \quad (65)$$

$$\begin{aligned} \bullet \int_{-\infty}^{\infty} dx \frac{e^{i a x}}{a^2 + x^2} &= \oint dz \frac{e^{i a z}}{(z + i a)(z - i a)} = 2\pi i \text{Res}_{z=i a} \left[ \frac{e^{i a z}}{(z + i a)(z - i a)} \right] \\ &= 2\pi i \lim_{z \rightarrow i a} \frac{e^{i a z}}{(z + i a)(z - i a)} (z - i a) = 2\pi i \frac{e^{-a x}}{2i a} = \frac{\pi e^{-a x}}{a} \quad (a > 0) \end{aligned} \quad (66)$$

$$\Rightarrow (65) = \sum_{\mathbf{q}_{\parallel}} \frac{e^2}{2\varepsilon \varepsilon_0 V_{\parallel}} e^{i \mathbf{q}_{\parallel} \mathbf{r}_{\parallel}} \frac{e^{-|\mathbf{q}_{\parallel}| |\mathbf{r}_{\perp}|}}{|\mathbf{q}_{\parallel}|} = \sum_{\mathbf{q}_{\parallel}} W_{\parallel}^{2D}(\mathbf{q}_{\parallel}, \mathbf{r}_{\perp}) e^{i \mathbf{q}_{\parallel} \mathbf{r}_{\parallel}} \quad (67)$$

$$\therefore W_{||}^{2D}(\mathbf{q}_{||}, z) = \frac{e^2}{2\varepsilon\varepsilon_0 V_{||}} \frac{e^{-|\mathbf{q}_{||}|z}}{|\mathbf{q}_{||}|}. \quad (68)$$

Include (68) back into (62) through (67) for 2D-case

$$\begin{aligned} W_{\mathbf{k}, \mathbf{k}', \mathbf{q}}^{\alpha\beta\gamma\delta} &= \int \int d\mathbf{r}_1 d\mathbf{r}_2 u_{\mathbf{k}_{||}+\mathbf{q}_{||}}^{\alpha\dagger}(\mathbf{r}_1) u_{\mathbf{k}'_{||}-\mathbf{q}_{||}}^{\beta\dagger}(\mathbf{r}_2) V^{3D}(\mathbf{r}_2 - \mathbf{r}_1) e^{i\mathbf{q}_{||}(\mathbf{r}_2-\mathbf{r}_1)} u_{\mathbf{k}'_{||}}^{\gamma}(\mathbf{r}_2) u_{\mathbf{k}_{||}}^{\delta}(\mathbf{r}_1) \\ &= \frac{e^2}{2\varepsilon\varepsilon_0 V_{||}} \sum_{\mathbf{q}'_{||}} \int \int d\mathbf{r}_1 d\mathbf{r}_2 u_{\mathbf{k}_{||}+\mathbf{q}_{||}}^{\alpha\dagger}(\mathbf{r}_1) u_{\mathbf{k}'_{||}-\mathbf{q}_{||}}^{\beta\dagger}(\mathbf{r}_2) e^{i\mathbf{q}'_{||}(\mathbf{r}_2-\mathbf{r}_1)} \frac{e^{-|\mathbf{q}'_{||}|z_2-z_1}}{|\mathbf{q}'_{||}|} e^{i\mathbf{q}_{||}(\mathbf{r}_2-\mathbf{r}_1)} u_{\mathbf{k}'_{||}}^{\gamma}(\mathbf{r}_2) u_{\mathbf{k}_{||}}^{\delta}(\mathbf{r}_1), \end{aligned} \quad (69)$$

We take the limit  $z_1, z_2 \rightarrow 0$ , therefore the  $W_{\mathbf{k}, \mathbf{k}', \mathbf{q}}^{\alpha\beta\gamma\delta}$  take the form:

$$W_{\mathbf{k}, \mathbf{k}', \mathbf{q}}^{\alpha\beta\gamma\delta} = \frac{e^2}{2\varepsilon\varepsilon_0 V_{||}} \sum_{\mathbf{q}} \frac{1}{|\mathbf{q}|} \langle u_{\mathbf{k}+\mathbf{q}}^{\alpha} | u_{\mathbf{k}}^{\delta} \rangle \langle u_{\mathbf{k}'-\mathbf{q}}^{\beta} | u_{\mathbf{k}'}^{\gamma} \rangle \quad (70)$$

## C Motion Equation

We consider Hamiltonian (35), using Heisenberg motion equation part by part with creation and annihilation operator satisfies (26):

$$\begin{aligned}
[H_{1e}^0, c_{\alpha\mathbf{k}}^\dagger c_{\beta\mathbf{k}}] &= \sum_{\mathbf{k}'\lambda} \varepsilon_{\lambda,\mathbf{k}'} [c_{\lambda\mathbf{k}'}^\dagger c_{\lambda\mathbf{k}'} c_{\alpha\mathbf{k}}^\dagger c_{\beta\mathbf{k}}] \\
&= \sum_{\mathbf{k}'\lambda} \varepsilon_{\lambda,\mathbf{k}'} (c_{\lambda\mathbf{k}'}^\dagger c_{\lambda\mathbf{k}'} c_{\alpha\mathbf{k}}^\dagger c_{\beta\mathbf{k}} - c_{\alpha\mathbf{k}}^\dagger c_{\beta\mathbf{k}} c_{\lambda\mathbf{k}'}^\dagger c_{\lambda\mathbf{k}'}) \\
&= \sum_{\mathbf{k}\lambda'} \varepsilon_{\lambda,\mathbf{k}} (c_{\lambda\mathbf{k}}^\dagger \delta_{\lambda\alpha} \delta_{\mathbf{k}\mathbf{k}'} c_{\beta\mathbf{k}} - c_{\lambda\mathbf{k}}^\dagger c_{\alpha\mathbf{k}}^\dagger c_{\lambda\mathbf{k}'} c_{\beta\mathbf{k}} - c_{\alpha\mathbf{k}}^\dagger \delta_{\beta\lambda} \delta_{\mathbf{k}\mathbf{k}'} c_{\lambda\mathbf{k}'} + c_{\alpha\mathbf{k}}^\dagger c_{\lambda\mathbf{k}'}^\dagger c_{\beta\mathbf{k}} c_{\lambda\mathbf{k}'}) \\
&= \sum_{\mathbf{k}\lambda'} \varepsilon_{\lambda,\mathbf{k}} (c_{\lambda\mathbf{k}}^\dagger \delta_{\lambda\alpha} \delta_{\mathbf{k}\mathbf{k}'} c_{\beta\mathbf{k}} - \cancel{c_{\alpha\mathbf{k}}^\dagger c_{\lambda\mathbf{k}'}^\dagger c_{\beta\mathbf{k}} c_{\lambda\mathbf{k}'}} - c_{\alpha\mathbf{k}}^\dagger \delta_{\beta\lambda} \delta_{\mathbf{k}\mathbf{k}'} c_{\lambda\mathbf{k}'} + \cancel{c_{\alpha\mathbf{k}}^\dagger c_{\lambda\mathbf{k}'}^\dagger c_{\beta\mathbf{k}} c_{\lambda\mathbf{k}'}}) \\
&= (\varepsilon_\alpha(\mathbf{k}) - \varepsilon_\beta(\mathbf{k})) c_{\alpha\mathbf{k}}^\dagger c_{\beta\mathbf{k}}
\end{aligned} \tag{71}$$

$$\begin{aligned}
[H^{e-L}, c_{\alpha\mathbf{k}}^\dagger c_{\beta\mathbf{k}}] &= \sum_{\lambda\lambda'} \mathbf{p}_{\lambda\lambda'}(\mathbf{k}') [c_{\lambda\mathbf{k}'}^\dagger c_{\lambda'\mathbf{k}'} c_{\alpha\mathbf{k}}^\dagger c_{\beta\mathbf{k}}] + \sum_{\lambda\mathbf{k}'} \left( \hbar\mathbf{k}' + \frac{e^2 A^2}{2m} \right) [\cancel{c_{\lambda\mathbf{k}'}^\dagger c_{\lambda\mathbf{k}'} c_{\alpha\mathbf{k}}^\dagger c_{\beta\mathbf{k}}}] \\
&= \sum_{\lambda\lambda'\mathbf{k}'} \mathbf{p}_{\lambda\lambda'}(\mathbf{k}') (c_{\lambda\mathbf{k}'}^\dagger c_{\lambda'\mathbf{k}'} c_{\alpha\mathbf{k}}^\dagger c_{\beta\mathbf{k}} - c_{\alpha\mathbf{k}}^\dagger c_{\beta\mathbf{k}} c_{\lambda\mathbf{k}'}^\dagger c_{\lambda'\mathbf{k}'}) \\
&= \sum_{\lambda\lambda'\mathbf{k}'} \mathbf{p}_{\lambda\lambda'}(\mathbf{k}') (c_{\lambda\mathbf{k}'}^\dagger \delta_{\lambda'\alpha} \delta_{\mathbf{k}\mathbf{k}'} c_{\beta\mathbf{k}} - c_{\lambda\mathbf{k}'}^\dagger c_{\alpha\mathbf{k}}^\dagger c_{\lambda'\mathbf{k}'} c_{\beta\mathbf{k}} - c_{\alpha\mathbf{k}}^\dagger \delta_{\beta\lambda} \delta_{\mathbf{k}\mathbf{k}'} c_{\lambda'\mathbf{k}'} + c_{\alpha\mathbf{k}}^\dagger c_{\lambda\mathbf{k}'}^\dagger c_{\beta\mathbf{k}} c_{\lambda'\mathbf{k}'}) \\
&= \sum_{\lambda\lambda'\mathbf{k}'} \mathbf{p}_{\lambda\lambda'}(\mathbf{k}') (c_{\lambda\mathbf{k}'}^\dagger \delta_{\lambda'\alpha} \delta_{\mathbf{k}\mathbf{k}'} c_{\beta\mathbf{k}} - \cancel{c_{\lambda\mathbf{k}'}^\dagger c_{\alpha\mathbf{k}}^\dagger c_{\lambda'\mathbf{k}'} c_{\beta\mathbf{k}}} - c_{\alpha\mathbf{k}}^\dagger \delta_{\beta\lambda} \delta_{\mathbf{k}\mathbf{k}'} c_{\lambda'\mathbf{k}'} + \cancel{c_{\alpha\mathbf{k}}^\dagger c_{\lambda\mathbf{k}'}^\dagger c_{\beta\mathbf{k}} c_{\lambda'\mathbf{k}'}}) \\
&= \sum_{\lambda} (\mathbf{p}_{\lambda\alpha}(\mathbf{k}) c_{\lambda\mathbf{k}}^\dagger c_{\beta\mathbf{k}} - \mathbf{P}_{\beta\lambda'}(\mathbf{k}) c_{\alpha\mathbf{k}}^\dagger c_{\lambda\mathbf{k}})
\end{aligned} \tag{72}$$

$$\begin{aligned}
[H^{Coulomb}, c_{\lambda\mathbf{k}''}^\dagger c_{\lambda'\mathbf{k}''}] &= \sum_{\mathbf{k},\mathbf{k}',\mathbf{q}} \sum_{\alpha\beta\gamma\delta} W_{\mathbf{k},\mathbf{k}',\mathbf{q}}^{\alpha\beta\gamma\delta} [c_{\alpha,\mathbf{k}+\mathbf{q}}^\dagger c_{\beta,\mathbf{k}'-\mathbf{q}}^\dagger c_{\gamma,\mathbf{k}} c_{\delta,\mathbf{k}'} c_{\lambda\mathbf{k}''}^\dagger c_{\lambda'\mathbf{k}''}] \\
&= \sum_{\mathbf{k},\mathbf{k}',\mathbf{q}} \sum_{\alpha\beta\gamma\delta} W_{\mathbf{k},\mathbf{k}',\mathbf{q}}^{\alpha\beta\gamma\delta} (c_{\alpha,\mathbf{k}+\mathbf{q}}^\dagger c_{\beta,\mathbf{k}'-\mathbf{q}}^\dagger c_{\gamma,\mathbf{k}} c_{\delta,\mathbf{k}'} c_{\lambda\mathbf{k}''}^\dagger c_{\lambda'\mathbf{k}''} - c_{\lambda\mathbf{k}''}^\dagger c_{\lambda'\mathbf{k}''} c_{\alpha,\mathbf{k}+\mathbf{q}}^\dagger c_{\beta,\mathbf{k}'-\mathbf{q}}^\dagger c_{\gamma,\mathbf{k}} c_{\delta,\mathbf{k}'}) \\
&\bullet \quad c_{\alpha,\mathbf{k}+\mathbf{q}}^\dagger c_{\beta,\mathbf{k}'-\mathbf{q}}^\dagger c_{\gamma,\mathbf{k}} c_{\delta,\mathbf{k}'} c_{\lambda\mathbf{k}''}^\dagger c_{\lambda'\mathbf{k}''} = c_{\alpha,\mathbf{k}+\mathbf{q}}^\dagger c_{\beta,\mathbf{k}'-\mathbf{q}}^\dagger c_{\gamma,\mathbf{k}} \delta_{\lambda,\delta} \delta_{\mathbf{k}',\mathbf{k}''} c_{\lambda'\mathbf{k}''} - c_{\alpha,\mathbf{k}+\mathbf{q}}^\dagger c_{\beta,\mathbf{k}'-\mathbf{q}}^\dagger c_{\gamma,\mathbf{k}} c_{\lambda\mathbf{k}''}^\dagger c_{\delta,\mathbf{k}'} c_{\lambda'\mathbf{k}''} \\
&= c_{\alpha,\mathbf{k}+\mathbf{q}}^\dagger c_{\beta,\mathbf{k}'-\mathbf{q}}^\dagger c_{\gamma,\mathbf{k}} \delta_{\lambda,\delta} \delta_{\mathbf{k}',\mathbf{k}''} c_{\lambda'\mathbf{k}''} - c_{\alpha,\mathbf{k}+\mathbf{q}}^\dagger c_{\beta,\mathbf{k}'-\mathbf{q}}^\dagger \delta_{\lambda\gamma} \delta_{\mathbf{k}\mathbf{k}''} c_{\delta,\mathbf{k}'} c_{\lambda'\mathbf{k}''} + \cancel{c_{\alpha,\mathbf{k}+\mathbf{q}}^\dagger c_{\beta,\mathbf{k}'-\mathbf{q}}^\dagger c_{\lambda\mathbf{k}''}^\dagger c_{\gamma,\mathbf{k}} c_{\delta,\mathbf{k}'} c_{\lambda'\mathbf{k}''}} \\
&\bullet \quad c_{\lambda\mathbf{k}''}^\dagger c_{\lambda'\mathbf{k}''} c_{\alpha,\mathbf{k}+\mathbf{q}}^\dagger c_{\beta,\mathbf{k}'-\mathbf{q}}^\dagger c_{\gamma,\mathbf{k}} c_{\delta,\mathbf{k}'} = c_{\lambda\mathbf{k}''}^\dagger \delta_{\lambda',\alpha} \delta_{\mathbf{k}'',\mathbf{k}+\mathbf{q}} c_{\beta,\mathbf{k}'-\mathbf{q}}^\dagger c_{\gamma,\mathbf{k}} c_{\delta,\mathbf{k}'} - \cancel{c_{\lambda\mathbf{k}''}^\dagger c_{\alpha,\mathbf{k}+\mathbf{q}}^\dagger c_{\lambda'\mathbf{k}''} c_{\beta,\mathbf{k}'-\mathbf{q}}^\dagger c_{\gamma,\mathbf{k}} c_{\delta,\mathbf{k}'}} \\
&= c_{\lambda\mathbf{k}''}^\dagger \delta_{\lambda',\alpha} \delta_{\mathbf{k}'',\mathbf{k}+\mathbf{q}} c_{\beta,\mathbf{k}'-\mathbf{q}}^\dagger c_{\gamma,\mathbf{k}} c_{\delta,\mathbf{k}'} - c_{\lambda\mathbf{k}''}^\dagger c_{\alpha,\mathbf{k}+\mathbf{q}}^\dagger \delta_{\lambda'\beta} \delta_{\mathbf{k}'',\mathbf{k}'-\mathbf{q}} c_{\gamma,\mathbf{k}} c_{\delta,\mathbf{k}'} + \cancel{c_{\lambda\mathbf{k}''}^\dagger c_{\alpha,\mathbf{k}+\mathbf{q}}^\dagger c_{\beta,\mathbf{k}'-\mathbf{q}}^\dagger c_{\lambda'\mathbf{k}''} c_{\gamma,\mathbf{k}} c_{\delta,\mathbf{k}'}} \\
[H^{Coulomb}, c_{\lambda\mathbf{k}''}^\dagger c_{\lambda'\mathbf{k}''}] &= \sum_{\mathbf{k},\mathbf{k}',\mathbf{q}} \sum_{\alpha\beta\gamma\delta} W_{\mathbf{k},\mathbf{k}',\mathbf{q}}^{\alpha\beta\gamma\delta} (c_{\alpha,\mathbf{k}+\mathbf{q}}^\dagger c_{\beta,\mathbf{k}'-\mathbf{q}}^\dagger c_{\gamma,\mathbf{k}} \delta_{\lambda,\delta} \delta_{\mathbf{k}',\mathbf{k}''} c_{\lambda'\mathbf{k}''} - c_{\alpha,\mathbf{k}+\mathbf{q}}^\dagger c_{\beta,\mathbf{k}'-\mathbf{q}}^\dagger \delta_{\lambda\gamma} \delta_{\mathbf{k}\mathbf{k}''} c_{\delta,\mathbf{k}'} c_{\lambda'\mathbf{k}''} \\
&\quad - c_{\lambda\mathbf{k}''}^\dagger \delta_{\lambda',\alpha} \delta_{\mathbf{k}'',\mathbf{k}+\mathbf{q}} c_{\beta,\mathbf{k}'-\mathbf{q}}^\dagger c_{\gamma,\mathbf{k}} c_{\delta,\mathbf{k}'} + c_{\lambda\mathbf{k}''}^\dagger c_{\alpha,\mathbf{k}+\mathbf{q}}^\dagger \delta_{\lambda'\beta} \delta_{\mathbf{k}'',\mathbf{k}'-\mathbf{q}} c_{\gamma,\mathbf{k}} c_{\delta,\mathbf{k}'})
\end{aligned}$$

$$\begin{aligned}
&= \sum_{\mathbf{k}, \mathbf{k}', \mathbf{q}} \sum_{\alpha \beta \gamma \delta} W_{\mathbf{k}, \mathbf{k}', \mathbf{q}}^{\alpha \beta \gamma \delta} c_{\alpha, \mathbf{k}+\mathbf{q}}^\dagger c_{\beta, \mathbf{k}'-\mathbf{q}}^\dagger c_{\gamma, \mathbf{k}} \delta_{\lambda, \delta} \delta_{\mathbf{k}', \mathbf{k}''} c_{\lambda' \mathbf{k}''} - \sum_{\mathbf{k}, \mathbf{k}', \mathbf{q}} \sum_{\alpha \beta \gamma \delta} W_{\mathbf{k}, \mathbf{k}', \mathbf{q}}^{\alpha \beta \gamma \delta} c_{\alpha, \mathbf{k}+\mathbf{q}}^\dagger c_{\beta, \mathbf{k}'-\mathbf{q}}^\dagger \delta_{\lambda \gamma} \delta_{\mathbf{k} \mathbf{k}''} c_{\delta, \mathbf{k}'} c_{\lambda' \mathbf{k}''} \\
&- \sum_{\mathbf{k}, \mathbf{k}', \mathbf{q}} \sum_{\alpha \beta \gamma \delta} W_{\mathbf{k}, \mathbf{k}', \mathbf{q}}^{\alpha \beta \gamma \delta} c_{\lambda \mathbf{k}''}^\dagger \delta_{\lambda', \alpha} \delta_{\mathbf{k}'', \mathbf{k}+\mathbf{q}} c_{\beta, \mathbf{k}'-\mathbf{q}}^\dagger c_{\gamma, \mathbf{k}} c_{\delta, \mathbf{k}'} + \sum_{\mathbf{k}, \mathbf{k}', \mathbf{q}} \sum_{\alpha \beta \gamma \delta} W_{\mathbf{k}, \mathbf{k}', \mathbf{q}}^{\alpha \beta \gamma \delta} c_{\lambda \mathbf{k}''}^\dagger c_{\alpha, \mathbf{k}+\mathbf{q}}^\dagger \delta_{\lambda' \beta} \delta_{\mathbf{k}'', \mathbf{k}'-\mathbf{q}} c_{\gamma, \mathbf{k}} c_{\delta, \mathbf{k}'} \\
&= \sum_{\mathbf{k}, \mathbf{q}} \sum_{\alpha \beta \gamma} W_{\mathbf{k}, \mathbf{k}'', \mathbf{q}}^{\alpha \beta \gamma \lambda} c_{\alpha, \mathbf{k}+\mathbf{q}}^\dagger c_{\beta, \mathbf{k}''-\mathbf{q}}^\dagger c_{\gamma, \mathbf{k}} c_{\lambda' \mathbf{k}''} - \sum_{\mathbf{k}', \mathbf{q}} \sum_{\alpha \beta \delta} W_{\mathbf{k}'', \mathbf{k}', \mathbf{q}}^{\alpha \beta \lambda \delta} c_{\alpha, \mathbf{k}''+\mathbf{q}}^\dagger c_{\beta, \mathbf{k}'-\mathbf{q}}^\dagger c_{\delta, \mathbf{k}'} c_{\lambda' \mathbf{k}''} \\
&- \sum_{\mathbf{k}', \mathbf{q}} \sum_{\beta \gamma \delta} W_{\mathbf{k}'', \mathbf{q}, \mathbf{k}', \mathbf{q}}^{\lambda' \beta \gamma \delta} c_{\lambda \mathbf{k}''}^\dagger c_{\beta, \mathbf{k}'-\mathbf{q}}^\dagger c_{\gamma, \mathbf{k}''-\mathbf{q}} c_{\delta, \mathbf{k}'} + \sum_{\mathbf{k}, \mathbf{q}} \sum_{\alpha \gamma \delta} W_{\mathbf{k}, \mathbf{k}', \mathbf{q}}^{\alpha \lambda' \gamma \delta} c_{\lambda \mathbf{k}''}^\dagger c_{\alpha, \mathbf{k}+\mathbf{q}}^\dagger c_{\gamma, \mathbf{k}} c_{\delta, \mathbf{k}''+\mathbf{q}} \\
&= \sum_{\mathbf{k}, \mathbf{q}} \sum_{\alpha \beta \gamma} W_{\mathbf{k}, \mathbf{k}'', \mathbf{q}}^{\alpha \beta \gamma \lambda} c_{\alpha, \mathbf{k}+\mathbf{q}}^\dagger c_{\beta, \mathbf{k}''-\mathbf{q}}^\dagger c_{\gamma, \mathbf{k}} c_{\lambda' \mathbf{k}''} - \sum_{\mathbf{k}', \mathbf{q}} \sum_{\alpha \beta \delta} W_{\mathbf{k}'', \mathbf{k}', \mathbf{q}}^{\alpha \beta \lambda \delta} c_{\alpha, \mathbf{k}''+\mathbf{q}}^\dagger c_{\beta, \mathbf{k}'-\mathbf{q}}^\dagger c_{\delta, \mathbf{k}'} c_{\lambda' \mathbf{k}''} \\
&- \sum_{\mathbf{k}', \mathbf{q}} \sum_{\beta \gamma \delta} W_{\mathbf{k}'', \mathbf{q}, \mathbf{k}', \mathbf{q}}^{\lambda' \beta \gamma \delta} c_{\lambda \mathbf{k}''}^\dagger c_{\beta, \mathbf{k}'-\mathbf{q}}^\dagger c_{\gamma, \mathbf{k}''-\mathbf{q}} c_{\delta, \mathbf{k}'} + \sum_{\mathbf{k}, \mathbf{q}} \sum_{\alpha \gamma \delta} W_{\mathbf{k}, \mathbf{k}', \mathbf{q}}^{\alpha \lambda' \gamma \delta} c_{\lambda \mathbf{k}''}^\dagger c_{\alpha, \mathbf{k}+\mathbf{q}}^\dagger c_{\gamma, \mathbf{k}} c_{\delta, \mathbf{k}''+\mathbf{q}} \\
&= 2 \sum_{\mathbf{k}' \mathbf{q}} \left( \sum_{\alpha \beta \gamma} W_{\mathbf{k}'', \mathbf{k}', \mathbf{q}}^{\alpha \beta \gamma \lambda} c_{\alpha \mathbf{k}''+\mathbf{q}}^\dagger c_{\beta \mathbf{k}'-\mathbf{q}}^\dagger c_{\gamma \mathbf{k}'} c_{\lambda' \mathbf{k}''} + W_{\mathbf{k}', \mathbf{k}''+\mathbf{q}, \mathbf{q}}^{\alpha \lambda' \gamma \delta} c_{\lambda \mathbf{k}''}^\dagger c_{\alpha \mathbf{k}'+\mathbf{q}}^\dagger c_{\gamma \mathbf{k}''+\mathbf{q}} c_{\delta \mathbf{k}'} \right) \quad (73)
\end{aligned}$$

Using approximation for the 4-operators into the form of multiplication of 2-operators (Hartree-Fock approximation):

$$\begin{aligned}
\sum_{\mathbf{k}' \mathbf{q}} \left\langle c_{\alpha \mathbf{k}''+\mathbf{q}}^\dagger c_{\beta \mathbf{k}'-\mathbf{q}}^\dagger c_{\gamma \mathbf{k}'} c_{\lambda' \mathbf{k}''} \right\rangle &= - \sum_{\mathbf{k}' \mathbf{q}} \left\langle c_{\alpha \mathbf{k}''+\mathbf{q}}^\dagger c_{\gamma \mathbf{k}'} \right\rangle \left\langle c_{\beta \mathbf{k}'-\mathbf{q}}^\dagger c_{\lambda' \mathbf{k}''} \right\rangle \delta_{\mathbf{k}' \mathbf{k}''} \\
&= - \sum_{\mathbf{q}} \left\langle c_{\alpha \mathbf{k}''+\mathbf{q}}^\dagger c_{\gamma \mathbf{k}''+\mathbf{q}} \right\rangle \left\langle c_{\mathbf{k}''}^\dagger c_{\lambda' \mathbf{k}''} \right\rangle \quad (74)
\end{aligned}$$

$$\begin{aligned}
\sum_{\mathbf{k}' \mathbf{q}} \left\langle c_{\lambda \mathbf{k}''}^\dagger c_{\alpha \mathbf{k}'+\mathbf{q}}^\dagger c_{\gamma \mathbf{k}''+\mathbf{q}} c_{\delta \mathbf{k}'} \right\rangle &= \sum_{\mathbf{k}' \mathbf{q}} \left\langle c_{\lambda \mathbf{k}''}^\dagger c_{\delta \mathbf{k}'} \right\rangle \left\langle c_{\alpha \mathbf{k}'+\mathbf{q}}^\dagger c_{\gamma \mathbf{k}''+\mathbf{q}} \right\rangle \delta_{\mathbf{k}', \mathbf{k}''} \\
&= \sum_{\mathbf{q}} \left\langle c_{\lambda \mathbf{k}''}^\dagger c_{\delta \mathbf{k}''} \right\rangle \left\langle c_{\alpha \mathbf{k}''+\mathbf{q}}^\dagger c_{\gamma \mathbf{k}''+\mathbf{q}} \right\rangle \quad (75)
\end{aligned}$$

Include HFA (74) and (75) into (73). Take all the communication term (71), (72) and (73) into (39) to get the SBE in HFA:

$$\begin{aligned}
\frac{d}{dt} \rho_{\lambda \lambda'}(\mathbf{k}) &= - \frac{i}{\hbar} (\varepsilon_{\lambda}(\mathbf{k}) - \varepsilon_{\lambda'}(\mathbf{k})) \rho_{\lambda \lambda'} - \frac{ie}{\hbar m} \mathbf{A}(t) \sum_{\mu} (\mathbf{p}_{\lambda \mu}(\mathbf{k}) \rho_{\mu \lambda'}(\mathbf{k}) - \rho_{\lambda \mu}(\mathbf{k}) \mathbf{p}_{\mu \lambda'}(\mathbf{k})) \\
&+ \frac{i}{\hbar} (\Omega_{\lambda \mu}(\mathbf{k}) \rho_{\mu \lambda'}(\mathbf{k}) - \rho_{\lambda \mu}(\mathbf{k}) \Omega_{\mu \lambda'}(\mathbf{k})) \quad (76)
\end{aligned}$$

## D Dipole Matrix Elements

Starting from position matrix element:

$$\langle \psi_{\lambda \mathbf{k}} | \mathbf{r} | \psi_{\lambda' \mathbf{k}'} \rangle = \int \frac{d^3 r}{V} u_{\lambda \mathbf{k}}^*(\mathbf{r}) e^{-i \mathbf{k} \cdot \mathbf{r}} \mathbf{r} u_{\lambda' \mathbf{k}'}(\mathbf{r}) e^{i \mathbf{k}' \cdot \mathbf{r}} \quad (77)$$

$$\begin{aligned} &= i \nabla_{\mathbf{k}} \left( \int \frac{d^3 r}{V} e^{-i \mathbf{k} \cdot \mathbf{r}} u_{\lambda \mathbf{k}}^*(\mathbf{r}) u_{\lambda' \mathbf{k}'}(\mathbf{r}) e^{i \mathbf{k}' \cdot \mathbf{r}} \right) - \int \frac{d^3 r}{V} i e^{-i \mathbf{k} \cdot \mathbf{r}} (\nabla_{\mathbf{k}} u_{\lambda \mathbf{k}}^*) u_{\lambda' \mathbf{k}'} e^{i \mathbf{k}' \cdot \mathbf{r}} \\ &= i \nabla_{\mathbf{k}} \left( \frac{1}{N} \sum_i^N e^{i(\mathbf{k}' - \mathbf{k}) \cdot \mathbf{R}_i} \int_{V_{cell}} \frac{d^3 r}{V_{cell}} e^{-i \mathbf{k} \cdot \mathbf{r}} u_{\lambda \mathbf{k}}^*(\mathbf{r}) u_{\lambda' \mathbf{k}'}(\mathbf{r}) e^{i \mathbf{k}' \cdot \mathbf{r}} \right) \\ &\quad - i \frac{1}{N} \sum_i^N e^{i(\mathbf{k}' - \mathbf{k}) \cdot \mathbf{R}_i} \int_{V_{cell}} \frac{d^3 r}{V_{cell}} e^{i(\mathbf{k}' - \mathbf{k}) \cdot \mathbf{r}} (\nabla_{\mathbf{k}} u_{\lambda \mathbf{k}}^*) u_{\lambda' \mathbf{k}'}. \end{aligned} \quad (78)$$

Again, using the long-wavelength approximation to have

$$\langle \psi_{\lambda \mathbf{k}} | \mathbf{r} | \psi_{\lambda' \mathbf{k}'} \rangle \approx i \nabla_{\mathbf{k}} \delta_{\mathbf{k}, \mathbf{k}'} \delta_{\lambda \lambda'} - i \delta_{\mathbf{k}, \mathbf{k}'} \langle \nabla_{\mathbf{k}} u_{\lambda \mathbf{k}} | u_{\lambda' \mathbf{k}'} \rangle, \quad (79)$$

Define the dielectric matrix elements:

$$\xi_{\lambda \lambda'}(\mathbf{k}) = -i \langle \nabla_{\mathbf{k}} u_{\lambda \mathbf{k}} | u_{\lambda' \mathbf{k}'} \rangle, \quad (80)$$

Include this into (79) to have

$$\langle \psi_{\lambda \mathbf{k}} | \mathbf{r} | \psi_{\lambda' \mathbf{k}'} \rangle = \delta_{\mathbf{k}, \mathbf{k}'} (i \delta_{\lambda \lambda'} \nabla_{\mathbf{k}} + \xi_{\lambda \lambda'}(\mathbf{k})), \quad (81)$$

Using this relation along with (31) and  $[H_{1e}^0, \mathbf{r}] = -i \frac{\hbar}{m} \mathbf{p}$  for  $\lambda \neq \lambda'$ :

$$\xi_{\lambda \lambda'}(\mathbf{k}) = -\frac{i \hbar}{m} \frac{\mathbf{p}_{\lambda \lambda'}(\mathbf{k})}{\varepsilon_{\lambda}(\mathbf{k}) - \varepsilon_{\lambda'}(\mathbf{k})} \quad (82)$$